Chapter 7
Density Functional Theory Calculations of Enzyme–Inhibitor Interactions in Medicinal Chemistry and Drug Design

Alexander B. Rozhenko

Abstract The density functional theory (DFT) is currently predominating theoretical approach in quantum chemistry. It is suitable for investigating structures up to several hundreds of atoms, studying of reaction pathways and calculating precisely reaction energy values. The usage of the DFT approach for studying enzyme–substrate interactions could be a prospective way for elaborating new efficient enzyme inhibitors. This is a direct way to discovery of new drugs and modification of the existing drugs. While enzymes are still too large for the computational analysis using DFT, numerous efforts have been exerted in the last years in this field using simplified enzyme models or calculating for the substrate some valuable properties, important in the enzyme–substrate interactions. These examples have been analyzed in the current review. A rapid development of new efficient calculation routines makes it possible to increase the role of the DFT methods in medicinal chemistry in the nearest future.

Listing of Used Acronyms

ACE   angiotensin-converting enzyme
AChE   acetylcholinesterase
AD   Alzheimer's disease
AIDS   acquired immune deficiency syndrome
BACE-1 betasite of APP-cleaving enzyme-1
BChE   butyrylcholinesterase
Cat B   cathepsin B
DFT   density functional theory
DNA   deoxyribonucleic acid
EP   electrostatic potential

A. B. Rozhenko (✉)
Institute of Organic Chemistry, National Academy of Sciences of Ukraine,
Murmans'ka str. 5, Kyiv 02660, Ukraine
e-mail: a_rozhenko@ukr.net

EPS	electrostatic potential surface
FAAH	fatty acid amide hydrolase
FEP	free energy perturbation
HIV	human immunodeficiency virus
HMGR	3-hydroxy-3-methylglutaryl-coenzyme A reductase
HOMO	highest occupied molecular orbital
IC_{50}	half maximal inhibitory concentration
IEF	integral equation formalism
IN	integrase
LUMO	lowest unoccupied molecular orbital
MD	molecular dynamics
MD/MM	molecular mechanics/molecular dynamics
MEP	molecular electrostatic potential
MFCC	molecular fractionation with conjugate caps approach
MMP	matrix metalloproteinase
MNDO	modified neglect of diatomic overlap
MO	molecular orbital
MP2	second-order Møller-Plesset perturbation theory
PCM	polarizable continuum model
PDE	phosphodiesterase
PES	potential energy surfaces
PLA_2	phospholipases A_2 enzymes
PM3	parameterized model number 3 (Stewart's semi-empirical approach)
PMF	potential of mean force
QM/MM	quantum mechanic/molecular mechanics hybrid approach
QSAR	quantitative structure–activity relationship
RHF	restricted Hartree-Fock method
RI	resolution of the identity
RNA	ribonucleic acid
SCC-DFTB	self-consistent charge-density functional tight binding
SCRFPCM	self-consistent reaction field polarizable continuum model
SIBFA	sum of interactions between fragments *ab initio* computed
TSS	transition state structures
XO	xanthine oxidase

7.1   Introduction

Over the last few decades, quantum chemical calculations became a powerful alternative to experimental methods in medicinal and drug chemistry in creating novel drug candidates [1–3]. One of these modern approaches is based on elaboration of small molecules, binding to the active site of an enzyme and inhibiting the reaction catalyzed by the enzyme [4]. These chemical substances should also exhibit

an unique selectivity for the target enzyme and exert their biological effect at low doses. Nowadays, enzyme inhibition is one of the key approaches to the drug design in the research and industry [5]. As reported in the recent review devoted to drug predictions methods [6], the drugs using the enzymes as targets amount to 24 % from the total number of small-molecule medicaments. Currently the computational techniques and software have become suitable for the theoretical analysis of the enzyme–substrate interactions [2]. The molecular docking [7], based on the molecular mechanics/molecular dynamics techniques, and quantitative structure–activity relationship (QSAR) methods [8], are widely used for this purpose.

An efficient enzyme–inhibitor interaction is usually characterized by a negative free binding energy, ΔG. This is equivalent to the reaction free energy, widely used in the quantum chemical description of chemical processes. Therefore, a maximization of the enzyme–substrate negative interaction energy under control of classical quantum-mechanical methods, *ab initio* or density functional theory (DFT), would probably be the most direct way to discover new efficient drug substances and to modify the existing drugs. The detailed outlook of using the DFT for calculations of ligand–protein complexes is given in the recent review of Utkov et al. [9]. However, despite the rapid development observed in computational techniques and routines, the quantum-mechanical methods (*ab initio* and DFT approaches) are still too slow and size-restricted or too inexact (molecular mechanics or semi-empirical methods) to provide a quantitative description for kinetics and thermodynamics of enzyme inhibition processes. One way to overcome the size problem in DFT calculations is to consider the interactions with every amino acid in the polypeptide chain separately and then to sum all the contributions. This approach is realized, for example, in the molecular fractionation with conjugate caps (MFCC) approach [10, 11]. In the other approaches, such as QM/MM calculations [12–14] or ONIOM routine implemented in the Gaussian sets of programs [12], the DFT calculations are used only for the small fragments of the active site and inhibitor structure, whereas the other part is described semi-empirically or by a classic force field [15]. The enzyme–inhibitor interactions investigated by using QM/MM methods are analyzed in the several recent reviews [16–18]. DFT calculations of the enzyme inhibition processes can be also performed for the truncated (up to several hundreds atoms) enzyme binding sites [19]. Recently some important steps have been undertaken for the rapid development of DFT-based drug chemistry. First of all, several efficient linear-scaling techniques [20] such as the *Resolution of the Identity* (*RI*) [21–27] have been proposed as an efficient solution of the size problem by quantum chemistry calculations and implemented into several popular quantum mechanic program sets (see, for example Ref. [28, 29]). Other well known indirect applications of the DFT methods in medicinal chemistry and drug design should be mentioned here: (a) evaluation of structure, conformation and properties, which can directly correlate with the inhibition activity of a molecules-candidate, such as molecular orbitals (MOs) [30, 31], electron density distribution, dipole moments [32], electrostatic potential surfaces (EPS) [33–36] etc.; (b) calculations of properties of structures, subsequently used as descriptors for QSAR analysis [8, 31–39].

The current short review is not exhaustive in the field. It covers mainly the last five years and gives examples of successful using the DFT methods for elaborating new drugs based on enzyme–inhibitor interactions.

7.2 Enzyme–Substrate Interaction Modelling Using DFT Methods

7.2.1 *Hydrolase*

Fatty acid amide hydrolase (FAAH) catalyzes hydrolysis of several fatty acid amides, in particular, transforms arachidonoylethanolamide to arachidonic acid and ethanolamine. The FAAH inhibition has an attractive therapeutic effect for the treatment of several central nervous system disorders. The inhibition mechanisms for two efficient FAAH inhibitors, O-aryl carbamate (**1**) and piperidinyl/piperazinyl-arylurea (**2**), have been recently studied by Lodola et al. [40] using the QM/MM approach. These inhibitors carbamoylate the active-site nucleophile Ser241. The theoretical model included self-consistent charge-density functional tight binding (SCC-DFTB), the approximate density functional theory method as the quantum-mechanical part. For the crucial steps of deacylation and decarbamoylation reactions, potential energy surfaces (PESs) were calculated and compared to that for deacylation of FAAH by the acylated substrate oleamide. A carbamic group bound to Ser241 substantially increased the activation energy for the hydrolysis reaction. Moreover, the activation energy derived theoretically for **1** was lower than that found for **2**, which is in line with the experimentally found for **1** and **2** reversible and irreversible inhibition, respectively.

1   **2**
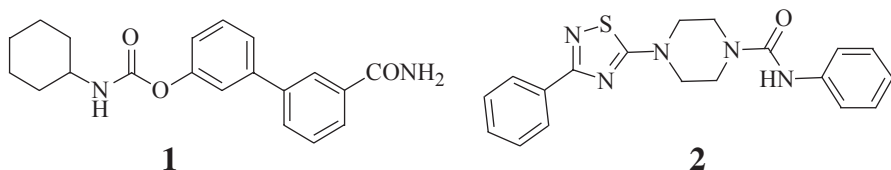
7.2.2 *APP-Cleaving Enzyme-1*

The betasite of APP-cleaving enzyme-1 (BACE-1) was used as target for the semi-empirical, DFT and MP2 calculations [41] for the adducts with a series of 14 hydroxyethylamines with a general formula **3** taken from Brookhaven Protein Data Bank. BACE-1 is a key enzyme in the production of Amyloid-β peptides, a major pathological feature of Alzheimer's disease [42, 43].

The interaction energy was determined for the complexes formed between the hydroxyethylamine as the BACE-1 inhibitors and 24 residues in the BACE-1 active

site. After a short molecular dynamics simulation the structures were optimized at the semiempirical level of theory. The optimized structures were used for single-point energy calculations with the M062X [44] and X3LYP DFT functional [45], which account for London dispersion forces, proper hydrogen-bonding and van der Waals complexes; alternatively the MP2 level of theory was employed. The active site cavity was separated into individual fragments to isolate each residue energy contribution when interacting with each ligand. The polar interactions were predominant in the system studied. In particular, the most remarkable role played the negatively charged aspartate residues with positively charged ligand moiety, providing a main contribution (over 90 %) to the total attractive interaction energy. On the other hand, the positively charged ARG296 residue exhibited the most repulsive ion–ion interaction that should also be reduced to improve the complex stability. The interactions with non-polar residuals, such as π,π-interactions, were less important, but taking them into account at the M062X or MP2 level of theory was required for providing better agreement with the experiment in the studied series of BACE-1 inhibitors.

3
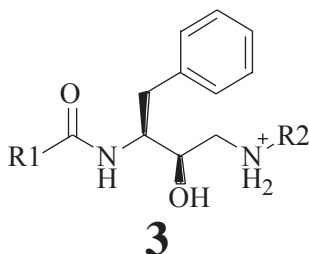
7.2.3   Reductase

A high level of cholesterol in blood (also called hypercholesterolaemia) [46] often cause the hardening and narrowing of arteries (atherosclerosis) in the major vascular systems. The cholesterol moderating statin drugs inhibit the second step in the biosynthetic pathway of producing cholesterol by binding to the active site of 3-hydroxy-3-methylglutaryl-coenzyme A reductase (HMGR), blocking the natural substrate of HMGR and disabling the synthesis of cholesterol [47]. Cafiero et al. [48] investigated theoretically (at the MP2 and DFT levels of theory) structures **4–7** and **8–10** (Fig. 7.1) – the products of modification of the existing drugs, the efficient HMGR inhibitors rosuvastatin and simvastatin, respectively. The rosuvastatin and simvastatin moieties interact with one end of the active site (Ser684, Asp690, Lys691 and Lys692), whereas the novel products bind to another end of the active site (Tyr479). The calculated interaction energies between Tyr479 and fragment **11** increased with increasing electron acceptor effects of the substituents X_1–X_3 (Table 7.1). The popular B3LYP DFT method was inadequate for this type of system and the local functional SVWN was used instead. The highest interaction

4-7

8-10

11
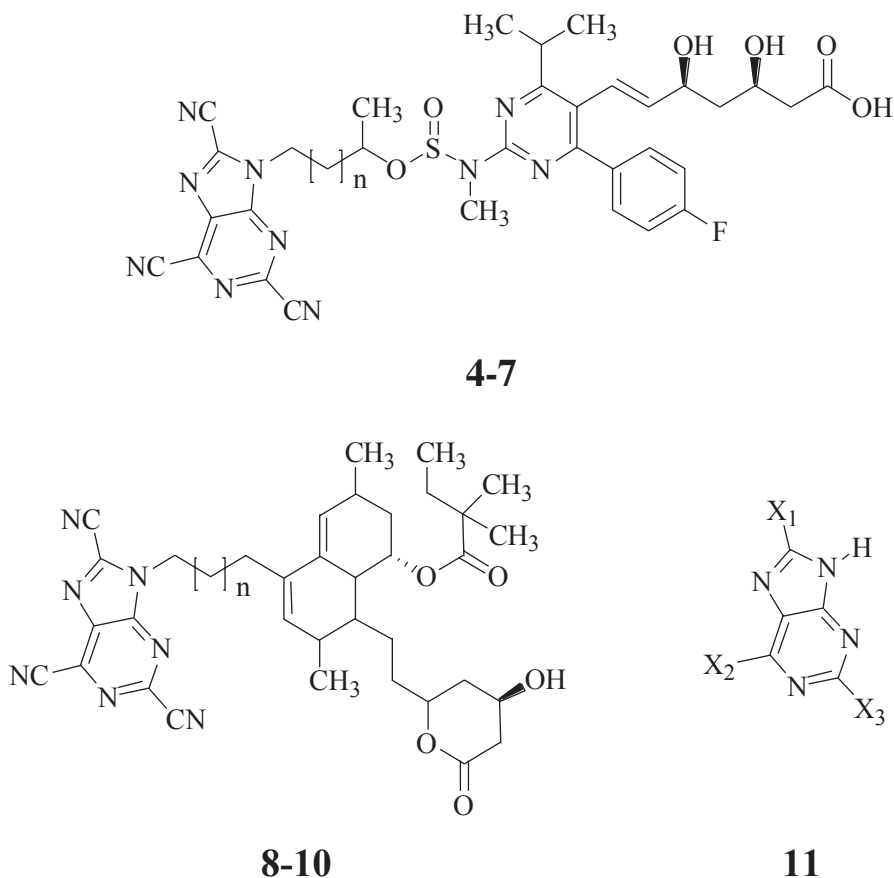
Fig. 7.1 Structure of drug candidates **4** (n=3), **5** (n=4), **6** (n=5), **7** (n=6), **8** (n=8), **9** (n=9) and **10** (n=10), and structure **11** as a novel drug fragment (see Table 7.1 for substituents X_1–X_3). (Reproduced with permission from Ref. [48]. Copyright © 2011 Elsevier)

Table 7.1 Counterpoise corrected interaction energies (kcal/mol) between Tyr479 and bicyclic fragment **11** by variation of the substituents X_1–X_3 (6-311++G(d,p) basis sets were used). (Reproduced with permission from Ref. [48]. Copyright © 2011 Elsevier)

Calc. method	NH_2 (X_1)	CN (X_2)	CN (X_1, X_2)	CN (X_3)	CN (X_1–X_3)	CN (X_1–X_3)	Cl (X_1–X_3)	NO_2 (X_1–X_3)
MP2	−5.45	−6.68	−8.51	−6.09	−7.94	−9.27	−8.46	−11.73
B3LYP	2.75	2.00	0.51	2.33	0.83	0.01	1.03	−3.48
SVWN	−4.31	−5.17	−6.75	−4.80	−6.34	−7.34	−6.55	−13.04

energies were predicted for X_1–X_3=NO_2, but it was not suitable for creating novel drug molecules because the bulky NO_2 group prevented the molecule's ability to penetrate the enzyme's cavity. The CN group was chosen as a good compromise for modifying the heterocyclic site.

Table 7.2 Interaction energies (kcal/mol) for novel candidate molecules with the HMG-CoA reductase active site calculated using DFT in combination with 6-311++G** basis sets and semi-empirical methods. (Reproduced with permission from Ref. [48]. Copyright © 2011 Elsevier)

	B3LYP	SVWN	HCTH407	AM1
HMG-CoA	−1.11	−39.93[3][a]	1.06	–
Rosuvastatin	−5.01	−31.51	−5.14	−106.14
4	−23.12	−57.72	−18.27	9.89
5	10.71	−26.84	12.78	5.40
6	19.18	−6.27	18.56	9.67
7	−74.22	−104.46	−73.45	−41.95
Simvastatin	−5.81	−27.64	−7.01	1.20
8	−14.43	−40.28	−14.00	−6.30
9	1.28	−32.46	1.89	−1531
10	−6.56	−29.82	−5.53	−4.70

[a] MP2 value for comparison is: −20.49 using 6-311+G* basis sets

The candidates **4–10** were docked in the active site of HMGR and then DFT and AM1 calculations were performed for the final structures of the molecules. The calculated interaction energy values (Table 7.2) indicated that the SVWN approach provided better agreement with the data obtained at the MP2 level of theory than the B3LYP and HCTH functionals.

The highest interaction energy was predicted for **7**: proton transfer occurs between the carboxyl group of **7** and NH_2 group of Lys692, leading to the very strong charge–charge interaction, whereas **1** reveals approximately twice a lower interaction energy. All three simvastatin-based candidates **8–10** seemed to interact stronger with HMGR than the original drug. Thus, the modified drugs might also possess higher efficacy.

Russo et al. [49] applied DFT for studying binding mode of flavonoids brutieridin (**12**) and melitidin (**13**). These structural analogs of statins, extracted from bergamot, inhibit HMGR, lower lipid concentration and cholesterol levels and reduce the risks of stroke [50]. Similarly to statins, brutieridin and melitidin were expected to interact effectively with the active site of the human HMGR enzyme. The active site of the enzyme was modeled starting from the X-ray structure of the adduct of simvastatin with HMGR. After the crude geometry optimization using the MD/MM simulation, the structure was truncated to the size suitable for the quantum chemical description (approx. 150 atoms) [51], considering only 17 amino acids and substituting some of them by more simple moieties. Also for modeling brutieridin and melitidin the smaller structures, **14** and **15** (Fig. 7.2) were utilized. The B3LYP/6-31+G* approach was used for geometry optimization. One H atom of each amino acid residue coming from the protein was kept frozen at its crystallographic position. The energy values were then defined more exactly at the B3LYP/6-311++G** level of approximation. The solvent effects were taken into account within the framework of Self Consistent Reaction Field Polarizable Continuum Model (SCRFPCM) using the IEF-PCM approach. The B3LYP-optimized structure of the HMGR complex with **14** is shown in Fig. 7.3a. The found binding energy (ΔE), not corrected
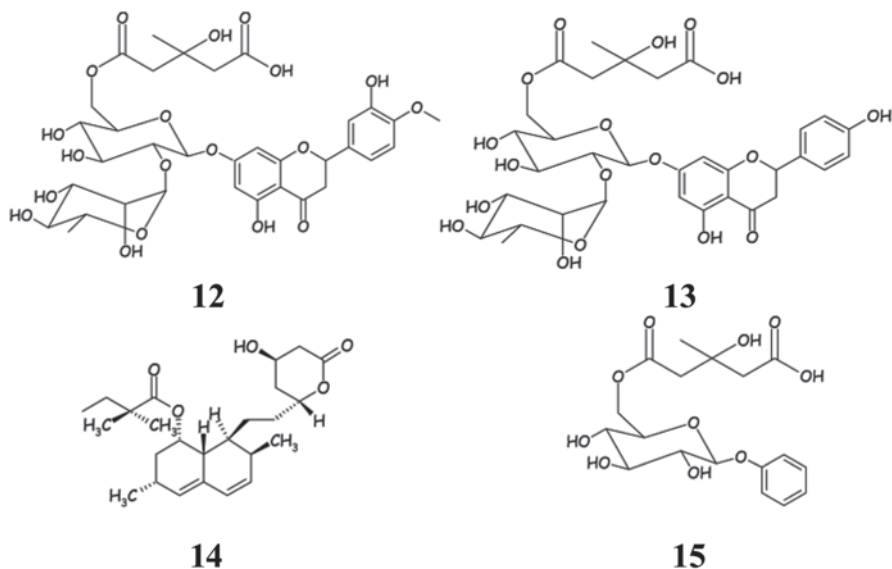
Fig. 7.2 Structures of brutieridin (**12**) and melitidin (**13**) and the model structures **14** and **15** used for calculations. (Reproduced with permission from Ref. [49]. Copyright © 2010 American Chemical Society)
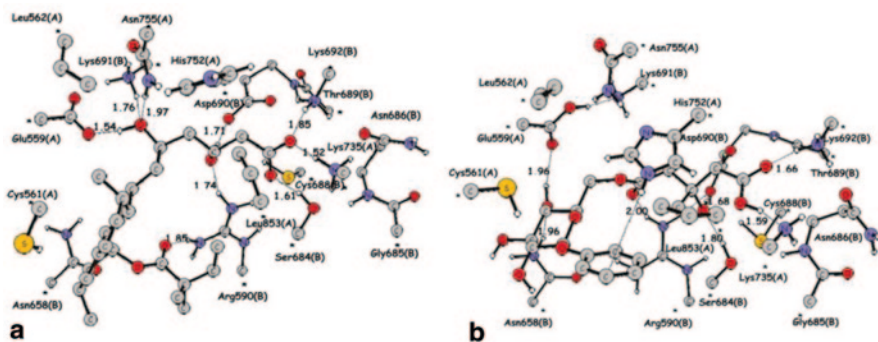
Fig. 7.3 B3LYP optimized geometry of the **3**-HMGR (*left*) and **4**-HMGR (*right*) complexes. For clarity, unimportant hydrogen atoms are omitted. (Reproduced with permission from Ref. [49]. Copyright © 2010 American Chemical Society)

for entropy effects, was rather high (−101.1 kcal/mol). The interactions in the adduct were mainly of electrostatic nature and include numerous hydrogen bonds. The equilibrium structure of the complex with **15** (Fig. 7.3b) was only slightly less favored ($\Delta E = -90.8$ kcal/mol). Therefore, **14** and **15** are good basis structures for a development of new anticholesterolemic drugs.

16-D   **16-L**   **17**

penicillin G, R=PhCH$_2$
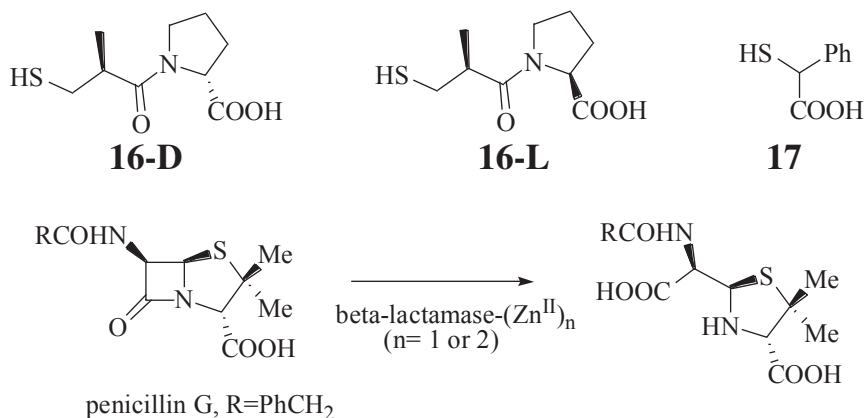
Scheme 7.1 Cleavage of the lactam ring of penicillin in presence of metallo-β-lactamase

7.2.4 *Metallo-β-lactamase*

The D- and L-captopril (**16**) [52] and D- and L-thiomandelate (**17**) [53], were studied theoretically as the simplified models for potential inhibitors of bacterial Zn^{2+} metallo-β-lactamase from *B. fragilis.* This enzyme cleaves the lactam ring of penicillin (Scheme 7.1), cephalosporin, and carbapenem antibiotics, strongly reducing their efficiency, which is a serious problem in medicine.

The theoretical investigations included molecular dynamics, SIBFA (Sum of Interactions Between Fragments *Ab initio* computed), molecular mechanics, HF and DFT calculations (on models of inhibitor–enzyme complexes on small model complexes including 88 atoms, extracted from the 104-residue complexes [53]. Calculations were carried out both with uncorrelated (HF) as well as correlated (DFT, MP2) quantum chemical approaches.

7.2.5 *Topoisomerase II and T7 RNA Polymerase*

Authors [54] studied the structure–activity relationship of four new polypyridyl ruthenium(II) complexes ([Ru(4dmb)$_2$(ppd)]$^{2+}$ (4dmb = 4,40-dimethyl-2,20-bipyridine, ppd = pteridino[6,7-f][1,10]phenanthroline-1,13(10H,12H)-dione) (**18**), [Ru(5dmb)$_2$(ppd)]$^{2+}$ (5dmb = 5,50-dimethyl-2,20-bipyridine) (**19**), [Ru(dip)$_2$(ppd)]$^{2+}$ (dip = 4,7-diphenyl-1,10-phenanthroline) (**20**), and [Ru(ip)$_2$(ppd)]$^{2+}$ (ip = imidazole[4,5-f][1,10]phenanthroline) (**21**)) as topoisomerase II and T7 RNA polymerase inhibitors and potential antitumor drugs. The frontier MOs were derived using the optimized geometries of the complexes. It was suggested that the lowest unoccupied MO (LUMO) provided a more effective overlap with the highest occupied MO (HOMO) of DNA. This correlated well with the DNA affinities of the

complexes, but the experimentally found trend of topoisomerase II inhibition activity was somewhat different from the DNA binding ability.

7.2.6 Cathepsin B Cysteine Protease

A series of organometallic compounds were studied using the DFT approach on the inhibitory properties against cathepsin B (cat B), a lysosomal papain-family cysteine protease [55]. Cat B is involved in cellular metabolism processes and implicated in the tumor progression and metastasis and hence it is the widely used target in medicinal chemistry. The Ru and Os complexes **22** and **23** and antimetastatic compound NAMI-A (**29**) showed similar enzyme inhibition properties *in vitro* (with IC_{50} values in the low µM range), whereas the Rh(III) and Ir(III) compounds (**24–28**) turned out to be inactive. As the direct coordination of the metal centre to the active site cysteine occurs, the different activities of the investigated organometallic complexes toward cat B were expected to be essentially determined by the strength of the corresponding covalent M–S bonds between the metal and cysteine residue. The authors used N-acetyl-L-cysteine-N′-methylamide ($CH_3CO–NH–CH(CH_2SH)–CO–NHCH_3$) as the model of cat B target, which mimics the cysteine side chain of the enzyme active site and neighboring peptide groups.


22, 23   **24, 25**   **26**

27   **28**   **29**
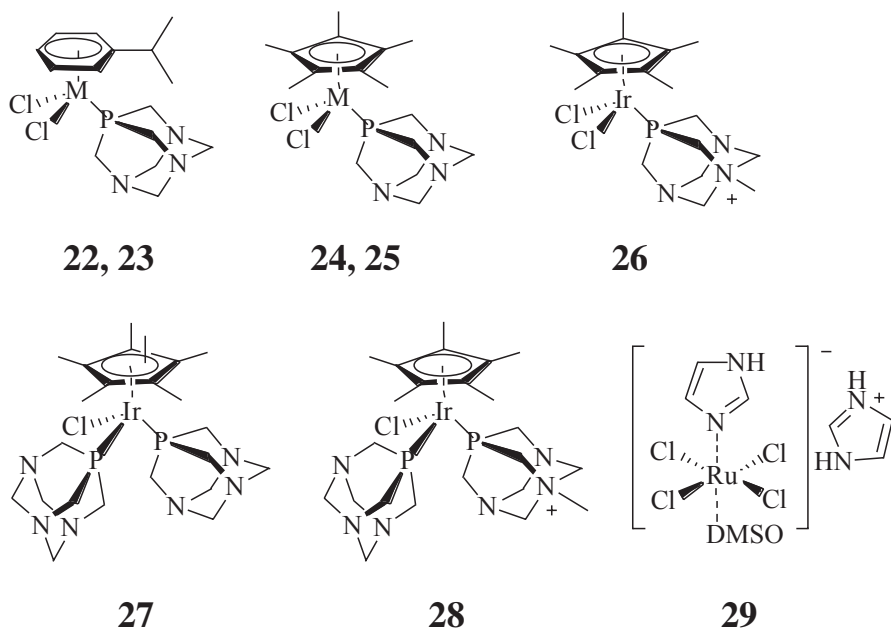
M= **22**: Ru, **23**: Os, **24**: Rh, **25**: Ir

The calculations predicted for some compounds thermodynamically favorable binding (negative ΔG values), whereas the inactive compounds were characterized by slightly positive binding free energy values. Thus, in contrast to Ru(II), Os(II) or Ru(III) complexes, the Rh(III) and Ir(III) compounds possessed a weak inhibition activity toward cat B, probably because the corresponding M–S bonds formed by these metal ions. They were characterized by *ca.* 20–30 kJ mol^{-1} lower bond energies than the more active complexes.

Shokhen et al. [56] analyzed possible mechanisms for the reversible formation of the complex between papain, a prototype enzyme of cysteine proteases, and peptidyl aldehyde inhibitors, using the quantum mechanical (DFT)/self consistent reaction field (virtual solvent) approach.

7.2.7 Acetylcholinesterase

Inhibitors of the acetylcholinesterase (AChE, E.C. 3.1.1.7) and butyrylcholinesterase (BChE, E.C. 3.1.1.8) activity demonstrate good results in the treatment of Alzheimer's disease (AD) [57, 58]. In the last years, the pathogenesis of AD has been associated with both cholinesterases, resulting in several studies that have targeted these two enzymes [59, 60]. Authors [61] investigated 88 N-aryl-substituted structures with general formulas **30** and **31** as potential inhibitors of the AChE and BChE residues using docking and density functional theory (DFT) methods. Some compounds were synthesized and their activities were tested *in vitro*. Among the candidates studied, several structures with the electron-acceptor substituents attached to the aromatic ring were predicted to be the most potent AChE inhibitors. These results demonstrated the importance of the electronic effects on ligand recognition and prompted authors to analyze HOMO and LUMO energies. They were suggested to correlate with biological activity [62]. The interaction between the aminoacids at the active site and inhibitors were considered to be determined by energies of frontier orbitals of the cholinesterase and substrate. This approach seems to be prospective for the design of new efficient AChE inhibitors.
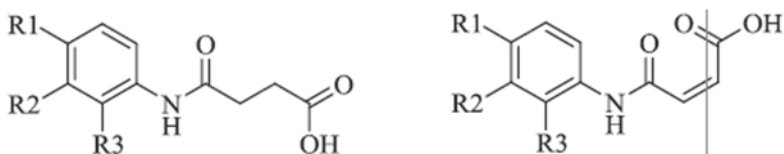
In the other work [63], semi-empirical, restricted Hartree-Fock (RHF) and DFT calculations were carried out to study the well-known acetylcholinesterase inhibitors tacrine (**32**), galantamine (**33**), donepezil (**34**), tacrine dimer (**35**), and physostigmine (**36**). Some electronic and structural properties were evaluated (Table 7.3),

Table 7.3 Electronic and geometrical parameters data for optimized AChEI structures by B3LYP/6-31+G(d,p) method. (Reproduced with permission from Ref. [63]. Copyright © 2008 Elsevier)

Property	32	33	34	35	36
HOMO (eV)	−5.76	−5.05	−5.95	−5.90	−5.46
Gap (eV)[a]	4.49	5.53	4.41	4.43	5.12
Volume ($Å^3$)	236	329	454	606	321
C–N (Å)	1.386	1.468	1.465	1.443	1.362
N–H (Å)	1.009	–	–	1.013	1.008
C–O (Å)	–	1.436	1.364	–	1.373
O–H (Å)	–	0.967	–	–	–
H–H (Å)	1.683	2.360	2.342	1.998	2.319
Charge H^+	0.30	0.34	0.15	0.26	0.32
Molecular size (E)	9.516	10.290	17.254	19.386	12.927

[a] Difference of energy between LUMO and HOMO orbitals

such as charge distribution, dipole moments, frontier orbital energies, acidity of hydrogens, molecular size, molecular volume, distance between the most acid hydrogens (H–H), and the molecular electrostatic potential (MEP). The calculated properties were used to correlate an inhibitory activity of the studied compounds towards acetylcholinesterase with their molecular structure.

Ganguly et al. analyzed the reaction of the sarin- [64] and VX-inhibited AChE [65] with nucleophiles by means of DFT [B3LYP/6-311G(d,p)] calculations. The hydroxylamine anion turned out to be more efficient in the reactivation process than other nucleophiles, for instance formoximate anion, and can be used as a good antidote agent against sarin and VX.

7.2.8 Matrix Metalloproteinases

Matrix metalloproteinases (MMPs) is a primary target for drug design, because it is involved in many biological processes, such as embryonic development [66], tissue remodeling and repair [67], neurophathic pain processes [68], cancers [69] [70], and other diseases. (4-Phenoxyphenylsulfonyl)methylthiirane also known as SB-3CT (**37b**) is the selective inhibitor of matrix metalloproteinase 2 (MMP2). The coupled deprotonation and ring-opening mechanism of SB-3CT inhibition of MMP2 (Scheme 7.2) as well as by 4-(phenoxyphenylsulfinyl)methylthiiranes (**38b**, **39b**), the sulfoxide analogue of SB-3CT, was examined computationally using DFT and QM/MM approaches [71].

For the model structures **38a** and **39a**, the complete conformational analysis was performed at the DFT (B3LYP/6-31+G(d)) level of theory. Nine conformational minima were identified for **38a** with energy differences between 0.2 and 4.8 kcal/mol. For the concerted deprotonation/ring-opening reaction, five different transition state structures (TSS) were located for the (*R*, *R*) diastereomer **38a** with the barrier
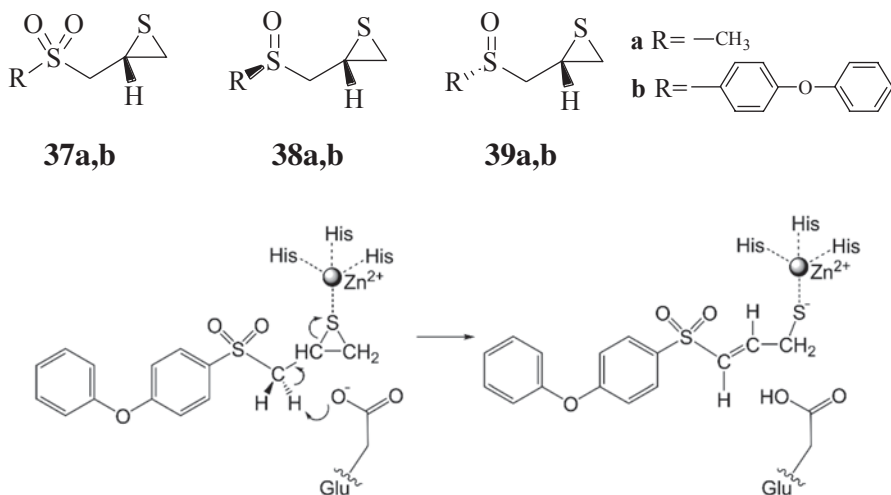
Scheme 7.2 Coupled deprotonation and ring-opening mechanism of the SB-3CT inhibition of MMP2. (Reproduced with permission from Ref. [71]. Copyright © 2010 American Chemical Society)

energies from 16.9 to 23.3 kcal/mol. For six located TSS for (*S, R*) diastereomer **39a** amplitudes of the relative energy variation was similar (from 16.9 to 22.0 kcal/mol). The lowest energies for the transition states turned out to be higher than that found for **37a**, modeling SB-3CT structure (16.9 *vs*. 11.3 kcal/mol, respectively). Therefore, the sulfoxide is less disposed to the concerted deprotonation/ring-opening reaction, probably due to the lower acidity of alkylarylsulfoxides compared with the corresponding sulfones.

Relative energies for the MMP2 complexes of **37b**, **38b** and **39b** (Fig. 7.4) were calculated using the ONIOM(B3LYP/6-311+G(d,p):AMBER) approach. In the active site of MMP2, the barriers for ring-opening for the sulfoxide analogues of SB-3CT (23.3 kcal/mol for **38b** and 28.5 kcal/mol for **39b**) were higher than that for SB-3CT (19.9 kcal/mol) [72], and overall the reactions for **38b** and **39b** (−17.2 and −17.3 kcal/mol, respectively) were less favored than that for SB-3CT (−21.0 kcal/mol), both kinetically and thermodynamically. The sulfoxide analogue of SB-3CT was found to be a linear competitive inhibitor, whereas SB-3CT itself was classified as a slow binding inhibitor.

One more important aspect of using the MMP inhibitors as drugs is their specific inhibition of one of 25 MMPs known in humans, or at least of one specific subgroup of this family of enzymes [73]. Guillaume et al. [74] reported a DFT (B3LYP/6-31G**+LANL2DZ) study for a series of potentially efficient inhibitors of matrix metalloprotease (MMP), N-acetyl-N′-sulfonylhydrazides (**40–48**). N-acetohydroxamic acid (**49**) and N-phenylsufonylglycine (**50**) were used for comparison.
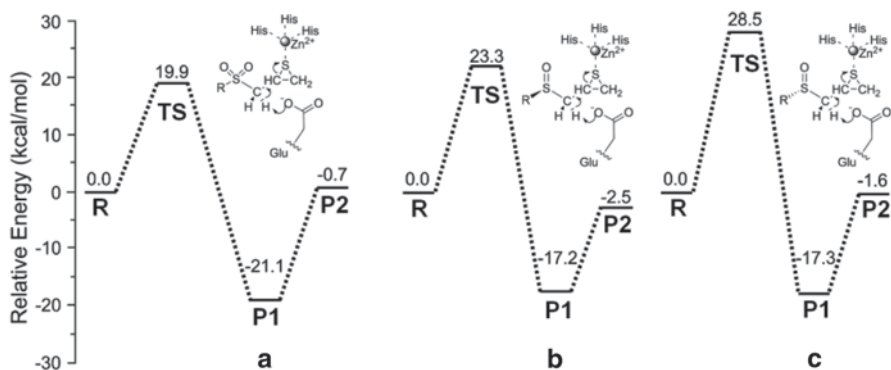
Fig. 7.4 Energy profiles for **37b** (**a**) and its sulfoxide analogues **38b** (**b**) and **39b** (**c**) in the MMP2 active site. R: reagents, TS: transition state, P1: products 1, P2: products 2. (Reproduced with permission from Ref. [71]. Copyright © 2010 American Chemical Society)


40-48   **49**   **50**
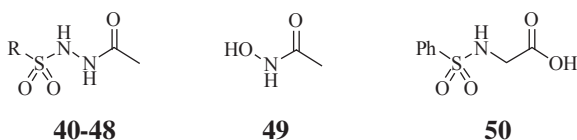
R: **40** Me; **41** Ph; **42** 4-MeC$_6$H$_4$; **43** 4-PhC$_6$H$_4$; **44** 4-PhOC$_6$H$_4$; **45** 4-FC$_6$H$_4$; **46** 3-NO$_2$C$_6$H$_4$; **47** 2-NO$_2$C$_6$H$_4$; **48** 2,4,6-(i-Pr)$_3$C$_6$H$_2$

The authors [74] evaluated the zinc-binding ability of ligands in an enzyme active site model composed of a Zn^{2+} ion using the DFT level of theory. Three main types of Zn–ligand interactions were found in the series of complexes studied. Type I corresponded to a bidentate zinc coordination involving the oxygen of the carbonyl group and the sulfonamide nitrogen atom. Type II resulted from an additional interaction with one of the sulfonyl oxygen atoms. As three 4-methylimidazole ligands were attached, the sulfamide nitrogen atom did not participate anymore in the complexation (the corresponding Zn–N distances were ~3.35 Å). Similar, but even more stable complexes were formed with a deprotonated form of the ligands.

A subsequent docking study resulted in the different coordination ability of **40–50** towards enzymes MM-1, MMP-2, MMP-9, MMP-12 and MMP-14 and demonstrated that these species can be used for the drug design as the efficient and selective MMP inhibitors.

Zhang and co-authors studied theoretically pyrogallic acid (**51**) and myricetin (**52**) as the potential non-peptide inhibitors of MMP-1 and MMP-3 [75]. The corresponding docked complexes with the model active sites were optimized at the B3LYP/6-31G* level of theory. Total calculated interaction energies for MMP-1 with **51** and **52** are −77.07 and −108.39 kcal/mol, respectively). Therefore, myricetin bound to MMP-1 more tightly than pyrogallic acid, which agreed with the
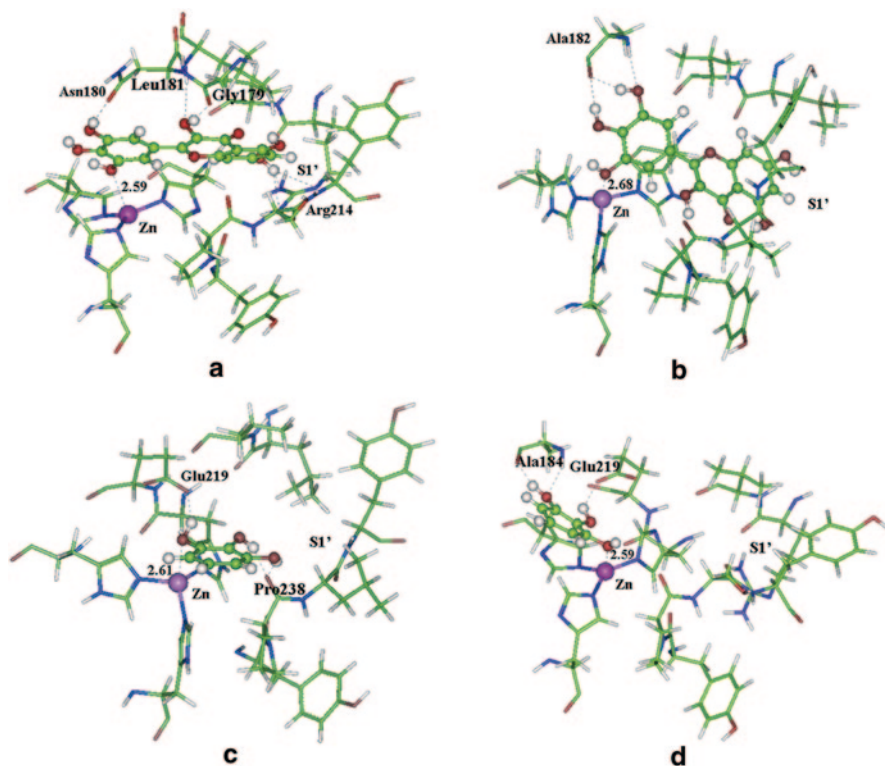
Fig. 7.5 Detailed representation of adducts of **51** (**a**, **c**) and **52** (**b**, **d**) adducts with MMP-1 (**a**, **b**) and MMP-3 (**c**, **d**) active sites. (Reproduced with permission from Ref. [73]. Copyright © 2011 Elsevier)

experimentally derived IC_{50} values for **51** and **52** (2.57 and 1.01 µM, respectively). The determined binding affinities with MMP-3 were found to be significantly lower (−52.37 and −74.56 kcal/mol, respectively), whereas the corresponding IC_{50} magnitudes were essentially higher (12.47 and 4.18 µM, respectively). Thus, **52** indicated better potency on both MMP-1 and MMP-3 than pyrogallic acid. The authors explained such result by a favorable interaction of the S′ cavity in the both MMPs with the benzopyran-4-one substituent in adducts of MMPs with **52** (Fig. 7.5), whereas by binding with **51** it remained empty.

**51**   **52**
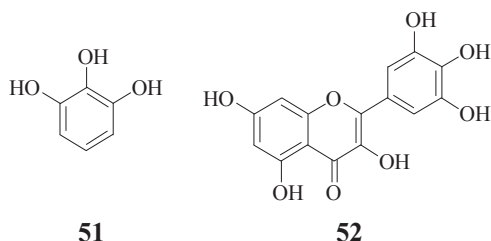
7.2.9 Phospholipases

The phospholipases A_2 (PLA$_2$) enzymes are responsible for the hydrolysis of membrane phospholipids that release arachidonic acid. The latter serves as substrate for pro-inflammatory mediators, such as prostaglandins and leucotriens. Inhibition of the enzymatic activity and edema induction by (PLA$_2$), extracted from the venom of *Crotalus adamanteus,* was explored by da Silva et al. [76]. Five different polyhydroxy phenolic compounds **53–57** were studied, both theoretically and experimentally, as the potential PLA$_2$ inhibitors. Molecular mechanics optimization indicated that the substrate binding occurred mainly via Asp49. This destabilized the interaction with calcium playing an important role in the catalytic activity of PLA$_2$. The electrostatic potential surface (EPS), calculated for compounds **53–57**, explained differences in inhibition of enzymatic activity of PLA$_2$: compounds **53–55** possessed the positive EPSs (approx. 0.7 eV) favorable for the formation of complexes with PLA$_2$. Compound **56** indicated the even higher positive magnitude of EPS (0.912 eV), strengthening the formed complex. Compound **57**, showed the EPS around 0.7 eV, but the hydroxyl groups in this molecule were sterically hindered by acetyl group. This prevented the formation of the inhibitor complex with PLA$_2$. Both **55** and **57** formed internal hydrogen bonds between the hydroxyl from position 2 and the carbonyl group. Thus, structures **53** and **54** demonstrated the highest inhibition activity.

53	**54**	**55**	**56**	**57**
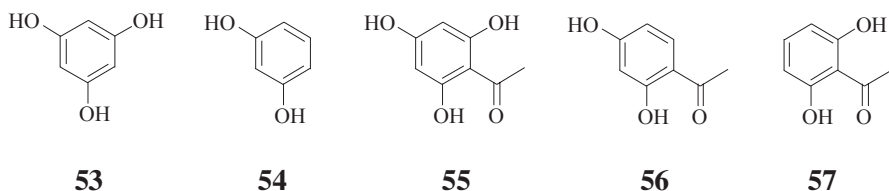
7.2.10 Angiotensin-Converting Enzyme

Šramko et al. investigated thermodynamics of the interaction of angiotensin-converting enzyme (ACE, EC 3.4.15.1) inhibitors with a truncated zinc metallopeptidase active site (Fig. 7.6) using DFT (B3LYP) and two-layered ONIOM B3LYP:MNDO approaches [77]. The authors investigated binding of various ACE inhibitors with $[Zn^{2+}(imidazole)_2 CH_3 COO^-]^+$ as the model binding site of ACE in neutral and anionic forms and calculate interaction and dissociation enthalpies and Gibbs energies (see Table 7.4). Several tested inhibitors were widely used drugs, effective in the treatment of hypertension, congestive heart failure, post-myocardial infarction and diabetic nephropathy [78], whereas the other ones were products of their structural modification. The 6-31+G(d,p) basis set was used for zinc, the dissociating functional groups and their closest vicinity, and the standard 6-31G(d)
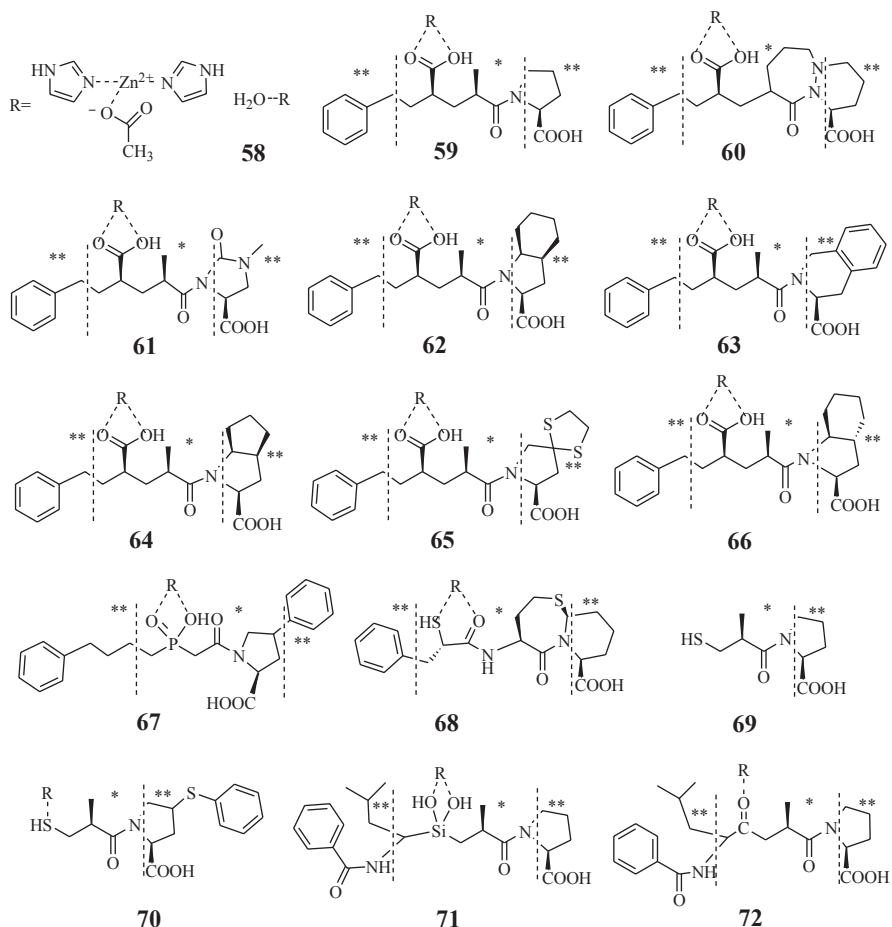
Fig. 7.6 Structural formulas of complexes of enzyme ("receptor") part (R) and neutral inhibitors with atom numbering. *Asterisks* exhibit different parts of molecules treated at the different levels of theory. (Reproduced with permission from Ref. [77]. Copyright © 2011 Elsevier)

basis sets were used for all the other atoms in the high layer. The ionized species originated by removal of proton from the acidic functional group of ACE inhibitor.

Complexes containing ionized (non-protonated) ACE inhibitors are marked with "**a**" and complexes containing neutral (protonated) ACE inhibitors are marked with "**b**". The structures of the optimized complexes **59a–66a** were very similar, with dissociated N-terminal carboxyl group of ACE inhibitors bound to zinc cation partially bidentately and acetate anion bound to zinc monodentately. Interestingly, the structural fragment of complex **59a** with inhibitor enalaprilat taken from Protein Data Bank (reference code 1UZE) was similar to the calculated structure, whereas in the optimized complex **69a** with inhibitor captopril, the inhibitor molecule was turned to the opposite side compared to the crystal structure (reference code 1UZF).

Table 7.4 Calculated gas-phase affinities of neutral ACE inhibitors to R expressed as interaction enthalpies, Gibbs Energies and entropies (at T=298 K). (Reproduced with permission from Ref. [73]. Copyright © 2011 Elsevier)
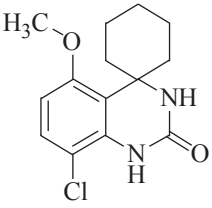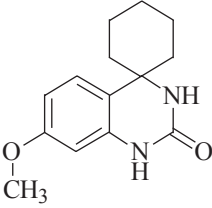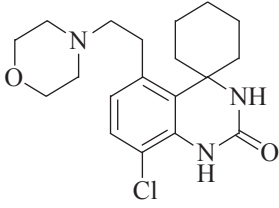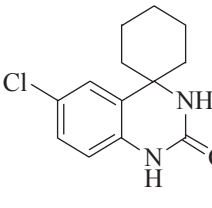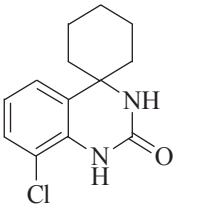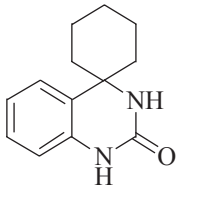
Complex	Inhibitor	ΔH^{298}	ΔG^{298}	ΔS^{298}	$\Delta\Delta G^{298}$
58b	H_2O	−13.56	−2.58	−36.82	0.0
59b	Enalaprilat	−22.07	−10.57	−38.60	−7.99
60b	Cilazaprilat	−23.21	−11.93	−37.82	−9.36
61b	Imidaprilat	−23.26	−11.78	−38.50	−9.20
62b	Perindoprilat	−21.31	−10.94	−34.78	−8.36
63b	Quinaprilat	−22.19	−11.20	−36.87	−8.62
64b	Ramiprilat	−21.80	−10.59	−37.60	−8.02
65b	Spiraprilat	−22.53	−11.68	−36.41	−9.10
66b	Trandolaprilat	−21.89	−10.95	−36.68	−8.37
67b	Fosinoprilat	−24.93	−11.92	−43.63	−9.35
68b	Omapatrilat	−17.68	−5.94	−39.38	−3.36
69b	Captopril	−14.85	−2.32	−42.03	0.25
70b	Zofenoprilat	−15.10	−3.25	−39.75	−0.67
71b	Silanediol	−13.67	−0.94	−42.71	1.64
72b	Keto-ACE	−21.07	−6.14	−50.07	−3.56

[a] Relative interaction Gibbs free energy values against water complex (**58b**)

In general, interaction enthalpies and Gibbs free energies of negatively charged ionic ACE inhibitors (Table 7.4) were significantly larger than those of neutral inhibitors (not shown here), but the acidity of the inhibitors considerably increases upon chelation: deprotonation Gibbs free energies (ΔG^{298}) of ACE inhibitors in complex with the model active site R were by the average of 85.96 kcal/mol lower than the deprotonation Gibbs energies of the free inhibitors. The results of the study [77] demonstrate that all structures within the investigated series are able to form stable tetra- or penta-coordinated complexes with R system. The highest binding affinity was observed for N-terminal anion of captopril ($\Delta G^{298}=−96.66$ kcal/mol). The model used was proven to be suitable for the analysis of the potential angiotensin-converting enzyme inhibitors and can be treated using DFT methods.

7.2.11 Phosphodiesterase

Inhibitory properties for series of 54 phosphodiesterase 7 (PDE7) inhibitors (spiroquinazolinones), previously reported by Lorthiois and coworkers [79, 80], was studied using docking and DFT methods with the aim of identifying the characteristics that distinguish between potent and weak inhibitors [81]. The conformations from docking studies were further used for DFT (B3LYP/6-31G*) geometry optimization. It is generally suggested that molecules with similar electrostatic potential (EP) surfaces may bind well to the same receptor [82–84]. The EPs calculated for the series of inhibitors (Fig. 7.7) were compared with the experimentally determined pIC_{50} magnitudes. The relative nucleophilicity of N1 with respect to N3 in

	73	74	75
EP(N1)	30.84;	42.81	28.93
EP(N3)	38.50	36.73	38.25
pIC$_{50}$	7.85	5.02	7.42

	76	77	78
EP(N1)	50.12	30.85	42.54
EP(N3)	38.45	38.22	36.53
pIC$_{50}$	5.32	6.77	5.18

Fig. 7.7 Structural formula, electrostatic potential values on N1 and N3 atoms (EP(N1) and EP(N3), respectively) and activity in molar concentration (pIC$_{50}$) for structures **73–78**

the spiroquinazolines was found to be important for the activity: all the active molecules had low EP(N1) and EP(N1) < EP(N3).

Thus, the electron density distribution in the molecules and steric factors are equally important for binding the molecules to the receptor. This computational study should aid in design of new molecules in this class with improved PDE7 inhibition.

7.2.12 HIV-1 Transcriptase

Searching for new effective anti-AIDS drug remains the challenge for drug chemistry [85]. One of the prospective ways is the development of efficient inhibitors of

the human immunodeficiency virus reverse transcriptase (HIV-1 RT). Authors [86] studied theoretically the binding of five different ligands **79–83** to the HIV-1 RT using molecular dynamics (MD) simulations within hybrid QM/MM potentials. Both potential of mean force (PMF) and free energy perturbation (FEP) methods presented **81** as the best candidate to inhibit the HIV-1 RT with binding energies −57.2 and −30.3 kcal/mol, respectively while for **83** the lowest negative binding energy was predicted (−16.4 and −9.0 kcal/mol, respectively). The EPS were derived from B3LYP/6-31+G(d,p) calculations. The active site displays the large positive electrostatic potential at the positions of the magnesium cations and nitrogen backbone atoms of Asp443, Glu478, Asp549 and His539, whereas the large negative regions were found at the positions of oxygen atoms of backbone belonging to His539, Asp443, Glu478, Asp498 and Asp549. The negative EP in the fragment of DNA-chain was at the oxygen atoms of the phosphate groups, hence there is a reasonable complementarity between the active site of the enzyme and its natural substrate.
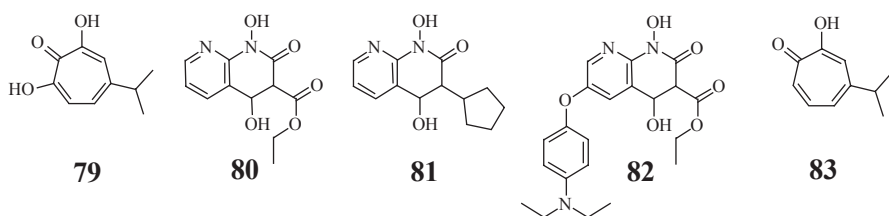
Liang and Chen [87] investigated the interaction between a potential anti-AIDS drug dapivirine and and the HIV-1 RT binding site using the ONIOM2 (B3LYP/6-31G(d,p): PM3) approach and calculating the energy at the B3LYP/6-31G(d,p) level of theory. The interaction energy was divided into several contributions coming from interactions with individual residues of the active site. The calculations predicted two hydrogen bonds between 2-aminopyrimidine groups of dapivirine with the carbonyl oxygen and amino hydrogen of Lys101. Additionally, two aromatic residues, Tyr181 and Tyr188, exhibited H···π and π···π interactions with the aromatic ring of dapivirine.

7.2.13 HIV-1 Aspartic Protease

Fleurat-Lessard et al. [88] analyzed the methods suitable for modeling human immunodeficiency virus type 1 aspartic protease (HIV-1 PR) enzyme. The semiempirical methods failed to describe the geometry of the protease active site. Within DFT, the best results were obtained with hybrid GGA B3LYP or X3LYP and with hybrid meta GGA functionals with a fraction of exact exchange around 30–40%, such as in the M06, B1B95, or BMK functionals. In the more recent work, Fleurat-Lessard et al. [89] studied using QM/MM method new HIV-1 drug candidates, potential inhibitors of HIV-1 PR. Though rigid structures are usually more efficient inhibitors of HIV-1 PR, they are less amenable to adapt to shape modifications of

the enzymatic binding site induced by mutations. Hasserodt et al. [90–92] proposed previously a new type of more mobile aspartic protease inhibitors, amino-aldehyde peptides, which adopted their form based on a non-covalent interaction of a tertiary amine nitrogen with a carbonyl group, the so-called N⋯CO bond. However, the calculations exhibited that the presence of water molecule W301 induced a systematic competition between formation/dissociation of the N⋯CO bond and the interaction network involving the structural water molecule. Probably, this competition determined the poor inhibition activity of amino-aldehyde peptides [90] and might be avoided by the proper design of non-peptidic cyclic hydrazino-urea derivatives.

Another way for the development of drugs using HIV-1 PR as target with minimizing the drug resistance effect of HIV-1 is an irreversible inhibition. It consists in the chemical modification of the binding site of HIV-1 PR, in particular, at the key Asp 25 and Asp25′ amino acid fragments resulted in the complete lost of catalytic activity. One possible way is to include the oxyrane ring in the potential drug structures [93–95]. Kóňa [96] analyzed two possible mechanisms of the irreversible inhibition of HIV-1 protease by epoxide inhibitors by means of *ab initio* (MP2) and DFT (B3LYP, MPW1K and M05-2X) calculations. In the first version of the reaction mechanism, the water molecule participated in the reaction, but another mechanism with a direct proton transfer from the acid catalyst to the inhibitor was shown to be more preferable. The structures (118 atoms) modeling both the local minima and transition state were located at the DFT [B3LYP/6-31+G(d,p)] level of theory. The activation energy was predicted to be *ca.* 15–21 kcal/mol. The process of irreversible inhibition exhibited significantly large negative reaction energy. The most probable mechanisms of modifying the model inhibitor structure were discussed.

7.2.14 HIV-1 Integrase

HIV-1 integrase (IN) is the relatively new and highly promising target for developing anti-AIDS drugs [97–99]. Understanding the inhibition mechanism of known inhibitors would make possible testing new perspective drug candidates using the DFT methods. However, it is still not known how the enzyme binds the inhibitors or its substrate, viral DNA [100]. The active site of HIV-1 IN is characterized by the dinuclear magnesium center, coordinated by carboxylate groups of three amino acid. Therefore, the main aim of theoretical efforts for the future development of the HIV-1 IN inhibitors with novel scaffolds is to provide a suitable ligand capable of chelating two Mg^{2+} ions [101]. Noteworthy, some efficient IN inhibitors exist in the multiple tautomeric forms [102], which were not studied in detail. Even less was known about the tautomerism of the ligands in the binding site of HIV-1 IN. The most stable tautomeric forms and rotamers for the known inhibitors of HIV-1 IN: α,γ-diketoacids (**84**), α,γ-diketotriazole (**85**), dihydroxypyrimidine carboxylate (**86**) and 4-quinolone-3-carboxylic acid (**87**) were calculated at the B3LYP/6-311++G(d,p) level of theory by Liao and Nicklaus [100]. Next, for the studied structures the chelating complexes with two magnesium ions in the moiety

modeling the active site of HIV-1 IN were calculated. As objects for DFT calculations, the magnesium ions were surrounded with three formic acids and four water molecules in order to mimic the IN binding site. In the optimized structures, the most stable forms in water solution included deprotonated, enolized or phenolic hydroxy groups, with the two eight-coordinated magnesium ions separated by a distance 3.70–3.74 Å. Replacing one water in the complex with one molecule of methanol mimiced the terminal 3′-OH of viral DNA, and the chelating complex remained stable. Probably, after 3′-processing, in the binding site of IN the terminal 3′-OH of viral DNA interacts with one Mg^{2+} by chelation.

84   **85**   **86**


87
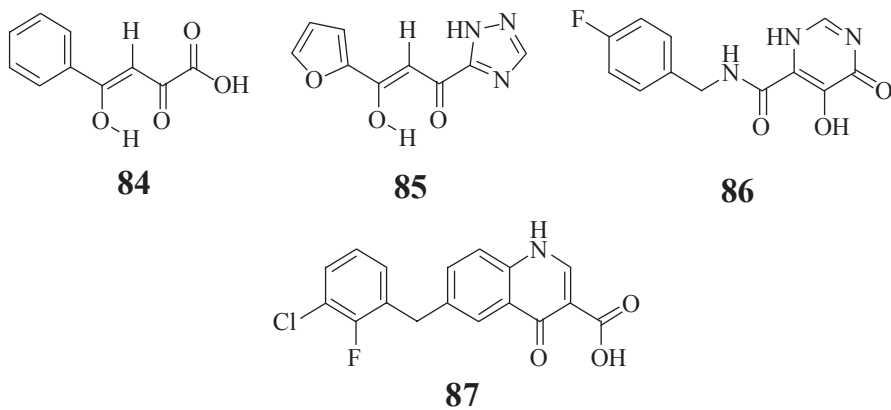
Wolschann et al. [103] used DFT calculations to identify the protonation state of HIV-1 IN, in particular, residues Lys156 and Lys159, which are of importance for binding 5CITEP inhibitor (**88**). The most favored conformations of 5CITEP were derived at the B3LYP/6-31G(d,p) level of theory by a variation of two torsion angles, Tor1 (C19-C11-C9-C8) and Tor2 (N3-C5-C6-C8) (Fig. 7.8, left). The potential energy surface (PES) was analyzed at the HF/3-21G level with subsequent reoptimization of the structures corresponding to local minima at the more superior B3LYP/6-31G(d,p) theoretical approach. The initial geometry of the IN/5CITEP adduct was taken from Protein Data Bank (PDB, entry code 1QS4). Interestingly, 5CITEP in the complex with IN in the X-ray determined structure, differs slightly from the equilibrium conformation of the free ligand, probably, due to additional interactions arising between 5CITEP and the surrounding amino acids.

Seven different structures of the complex were generated including both neutral and deprotonated forms of 5CITEP as well as both neutral and protonated forms of two lysines (Lys156 and Lys159) and then optimized by fixing the C_α atoms in the amino acids. The lowest energy structures for the protonated and non-charged states of the adduct are shown in Fig. 7.9. 5CITEP is in its neutral form, where the hydrogen atom is attached to N3 of the tetrazole ring while Lys156 and Lys159 are non-protonated and protonated, respectively. The structure of the
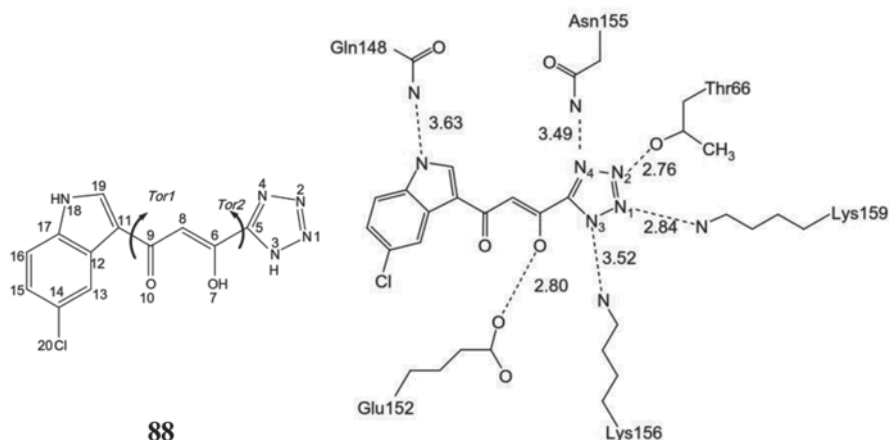
Fig. 7.8 Conformational analysis of 5CITEP (*left*); modeling the adduct of 5CITEP with the binding site of HIV-1 IN (*right*). (Reproduced with permission from Ref. [103]. Copyright © 2007 Elsevier)
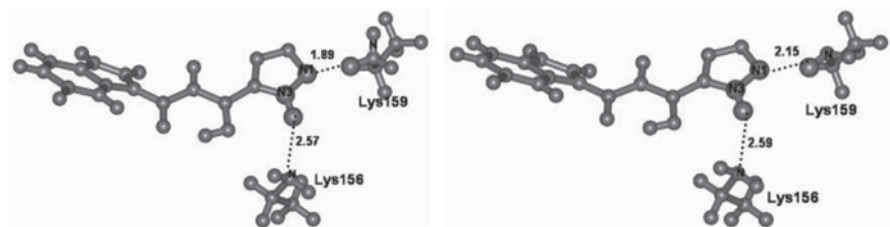

Fig. 7.9 The lowest energy configurations for the protonated (*left*) and non-charged (*right*) states of the adduct of **88** with Lys156 and Lys159 from HIV-1 IN. (Reproduced with permission from Ref. [103]. Copyright © 2007 Elsevier)

non-charged state is similar, but in contrast to the protonated form, both lysine residues are non-protonated.

For determining the binding energy, the most important six amino acids (Thr66, Gln148, Glu152, Asn155, Lys156, and Lys159) were selected (Fig. 7.8, right). Although the calculated structure of 5CITEP was slightly different from that found in the co-crystal structure, its binding energy (-41.33 kcal mol^{-1}) indicated the energetically favorable system. In contrast to the aforementioned adduct of 5CITEP with two lysine molecules (Lys156 and Lys159), in the complex including six amino acids, where the side chains of amino acids were allowed to change their position, proton at N3 of the ligand was transferred to Lys156.

Alves and co-authors [104] compared the activity of HIV-1 IN effective inhibitor S-1360 (**89**), that underwent clinical trials, with two its analogues **90** and **91**. While

the QM/MM calculations (using BLYP/6-31G* level for the QM region) predicted lower interaction energies for **90** and **91** (−611.7 and −622.7 kJ/mol) than for **89** (−667.0 kJ/mol), they exhibited strong interactions with the residues of the active site. The EP surfaces were analyzed for all three structures.
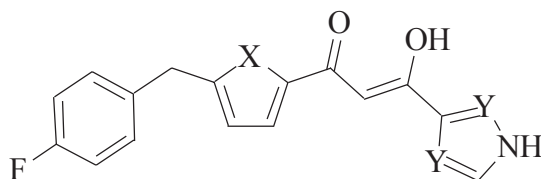
89: X=O, Y=N; **90** X=NH; Y=N; **91** X=O, Y=H

7.2.15   Xanthine Oxidase

Xanthine oxidase (XO) is a flavoprotein enzyme which catalyzes the oxidative hydroxylation of purine substrates. Because of its availability (it is abundant in cow's milk), XO has become a well-established target of drugs against gout and hyperuricemia. The reduction of molecular oxygen by XO produces free radicals which can cause damage to surrounding tissues. The activation of XO generates superoxide and hydrogen peroxide, hence it is generally seen as a potentially destructive agent in the vasculature. The paper of Lespade and Bercion [105] is devoted to the computational (DFT) study of one of the possible mechanisms of XO inhibition: the attraction and anchorage of the molecule inside the cavity. Two classes of potential inhibitors were tested as inhibitors: the series of flavonoids of natural origin [106, 107]: luteolin (**92**), apigenin (**93**), chrysin (**94**), kaempferol (**95**), galangin (**96**), myricetin (**97**), quercetin (**98**), morin (**99**); and gallic acid derivatives [108]: gallic acid (**100**), ellagic acid (**101**) and ellagic acid-4-*O*-*β*-D-xylopyranoside (**102**). For this purpose, electrostatic interactions between the molybdopterin moiety and two series of inhibitors were calculated at the DFT level of theory, in order to evaluate the interconnection between the electrostatic potential and inhibition forces. The most stable conformations were determined for the inhibitors using B3LYP/6-31+G(d,p) approach. As this functional poorly reproduces electron dispersion, the energies of the conformations were calculated at the MP2/6-31+G(d,p) level of theory. The authors of [105] concluded that the most potent inhibitors in the investigated series should be polar, possess a longitudinal dipole moment, and weakly dissociate at physiological pH.

7.2.16   Trombin

The activity of trombin is responsible for the cleavage of fibrogen to form fibrin that then polymerizes with forming a network of fibers. This determines not only

the positive wound-healing process, but also such diseases as myocardial infarction, pulmonary embolism and stroke [109]. Understanding the binding mechanism of the known inhibitors to thrombin would provide a valuable information for a discovery of new more efficient and selective inhibitors.
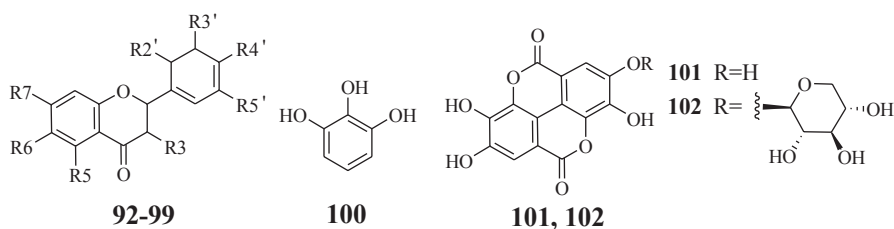

92 R3, R6,R2',R5'=H, R5, R7, R3', R4'=OH; **93** R3, R6, R2', R3', R5'= H, R5, R7, R4'= OH **94** R3, R6, R2', R3', R4', R5'=H, R5, R7=OH; **95** R6, R2', R3', R5'= H, R3, R5, R7, R4'= OH; **96** R6, R2', R3', R4', R5'= H, R3, R5, R7, = OH; **97** R6, R2', = H, R3, R5, R7, R3', R4', R5' = OH; **98** R6, R2', R5' = H, R3, R5, R7, R3', R4' = OH; **99** R6, R3', R5' = H, R3, R5, R7, R2', R4', = OH.

The authors [110] studied interactions of two pyrazinone- and prolyne-based macrocyclic inhibitors (**103** and **104**, respectively) using molecular dynamics simulations, DFT and molecular mechanics calculations. An analysis of binding interactions became possible by applying molecular fractionation with conjugate caps (MFCC) approach [10, 11]. In the case of **103** main binding attractions were provided by six residues with individual gas-phase binding energies > 2 kcal/mol: Ser[214], Trp[215], Gly[216], Glu[217], Asp[102], and Asp[189]. Similarly, for **104** interactions with Asp[189], Ser[214], Trp[215], Gly[216], Asp[102], and Glu[146] were of importance. The fragment interaction energies calculated at the MP2/6-311G* level of theory agreed well with those derived using the DFT (B3LYP/6-31G*) method. A good agreement was observed between the calculated and experimental binding free energy values.
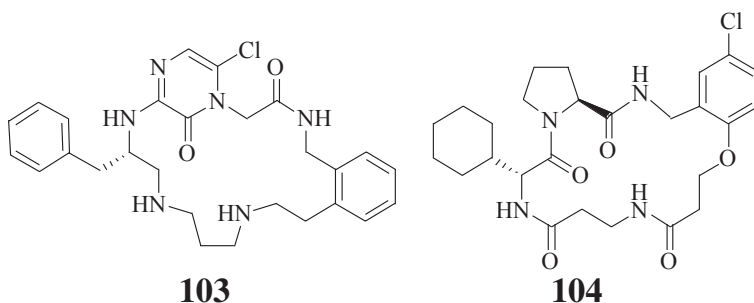
7.2.17 Lipase B

De Oliveira et al. [111] carried out quantum chemical (DFT) calculations for adducts of three flavonoids, quercetin (**98**), isoquercitrin (**105**) and rutin (**106**), docked in the mini-model that mimicked the catalytic site of *Candida antarctica* lipase B (CALB). The analysis of these results showed that an ester bond with the carbonyl C atom of the Ser105-bound acetate was expected for the rhamnose 4‴-O of rutin and for the glucose 6″-O of isoquercitrin, but no ester bond was predicted to be formed with the B-ring of 3′-O of quercetin. The mechanism of coordination was modeled calculating non-covalently bound as well as covalently bound intermediates. The theoretical results agreed well with the experiment.

105   **106**
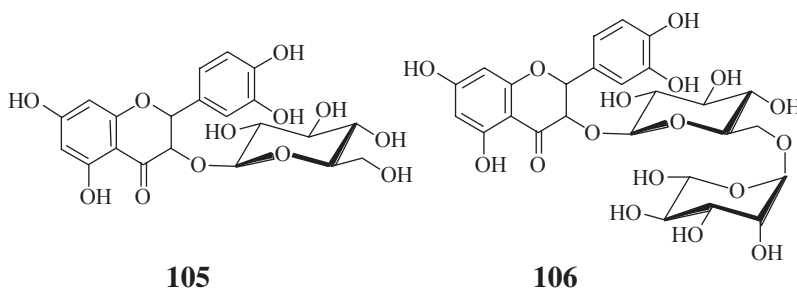
7.2.18 Urease

Urease (urea amidohydrolase, EC 3.5.1.5) is involved in a number of diseases, such as pyelonephritis, ammonia encephalopathy, hepatic coma, peptic ulcers and formation of kidney stones [112, 113], hence the urease inhibitors could be useful as efficient drugs. Leopoldini et al. [114] explored at the DFT (B3LYP using LANL2DZ basis set for Ni atoms and 6-311G** for all other atoms) boric acid as a rapid reversible inhibitor of urease. Two models of different size were analyzed. The smaller one included truncated amino acids from the first coordination shell of two Ni^{2+} ions: the histidine residues (His137, His139, His249, His275), the carbamylated lysine (Lys220) and the Asp363 were simulated by imidazole rings, a carboxylated methylamine (CH_3NHCOO^-) and an acetate group (CH_3COO^-) (Fig. 7.10). The B–O interactions were strong and possessed the covalent character. The bonding character did not change when the binding site model was extended by adding other amino acid residues and two water molecules involved in the inhibitor binding mode (totally 122 atoms). The boric acid molecule seemed to be firmly anchored to the enzyme and thus prevented the urease catalytic reaction.
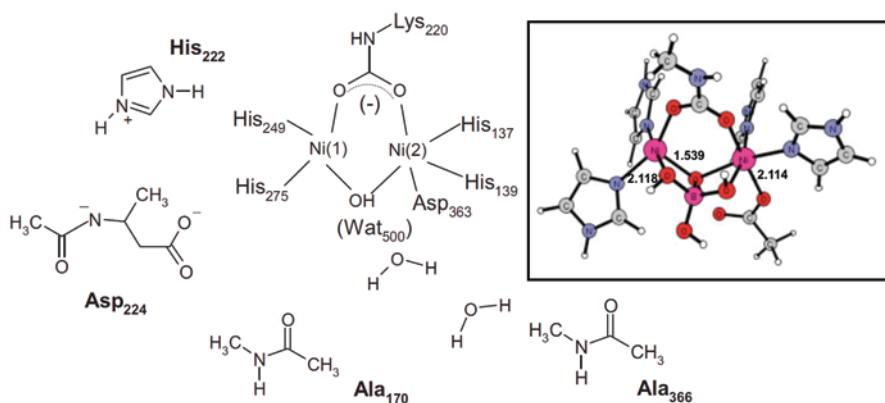
Fig. 7.10 Model used for the urease active site. The outer amino acids (*bold*) were added in the larger model. In the inset: optimized geometry of the complex of boric acid with the model of the urease binding site. The distances are in Å. (Reproduced with permission from Ref. [114]. Copyright © 2008 Wiley Periodicals, Inc.)

7.2.19 Other Results

Several 1,3-bisphospho-D-glyceric acid analogs were studied theoretically (using QM/MM molecular dynamics and DFT-based EPS) as potential inhibitors of glyceraldehyde-3-phosphate dehydrogenase, and as new drugs against Chagas disease [15]. The first detailed QM/MM study on the possible mechanisms for the reaction of proteasome with a representative peptide inhibitor, Epoxomicin was reported [115]. The obtained novel mechanistic insights should be valuable for a future rational design of more efficient proteasome inhibitors.

7.3 Conclusions and Prospects

The DFT approach is widely used nowadays in the pure form or in combination with other, less computationally demanding approaches for modeling enzyme–ligand adducts towards understanding mechanisms of enzyme catalyzed reactions and constructing novel drugs based on enzyme–inhibitor interactions. The recently developed efficient linear-scaling techniques like the *Resolution of the Identity (RI)* provide a new quantum chemical methodology for modeling ligand–protein interactions. Recently, the novel efficient linear-scaling methods have also been proposed for the hybrid functionals, such as the popular B3LYP [116, 117]. The frontiers of using DFT for modeling the enzyme–inhibitor interactions exceed now several hundreds atoms. This makes it possible to increase significantly the size of the DFT-calculated enzyme binding site fragments for the virtual (*in silico*) construction of the enzyme–inhibitor adducts. For example, the RI-DFT molecular dynamics

methods, RI-DFT-based geometry optimization and RI-MP2 single-point energy calculations can be combined for the model adducts of relatively large size. This gives us believe to assert that, similarly to quantum chemistry of small molecules, such kind of calculations will sooner or later turn into a routine.

Finally, the special event should be mentioned here as the scientific and public recognition of achievements of computational chemistry over the last decades and its great prospects in the future: the Nobel Prize in Chemistry 2013 awarded jointly to Martin Karplus, Michael Levitt and Arieh Warshel "for the development of multiscale models for complex chemical systems". Inter alia, the laureates laid the foundation for the modern QM/MM approach [118] based nowadays on the *ab initio* or DFT and MM/MD approaches. There is no doubt that the extent of the DFT constituent will grow, increasing the reliability of the method by modeling enzyme–inhibitor reactions.

References

1. Putz MV, Mingos DMP (eds) (2013) Applications of density functional theory to biological and bioinorganic chemistry. Springer, Berlin. doi:10.1007/978-3-642-32750-6
2. Dahan A, Khamis M, Agbaria R, Karaman R (2012) Targeted prodrugs in oral drug delivery: the modern molecular biopharmaceutical approach. Expert Opin Drug Del 9(8):1001–1013. doi:10.1517/17425247.2012.697055
3. Kortagere S (ed) (2013) In silico models for drug discovery: methods in molecular biology, vol 993. Humana Press, Totowa. doi:10.1007/978-1-62703-342-8
4. Jorgensen WL (2010) Drug discovery: pulled from a protein's embrace. Nature 466(7302):42–43. doi:10.1038/466042a
5. Sharma R (ed) (2012) Enzyme inhibition and bioapplications. InTech, Rijeka
6. Barril X (2012) Druggability predictions: methods, limitations, and applications. WIREs Comput Mol Sci. doi:10.1002/wcms.1134. doi:10.1002/wcms.1134
7. Morris GM, Lim-Wilby M (2008) Molecular docking. In: Methods in molecular biology. Spinger, Clifton, p 365–382
8. Puzyn T, Leszczynski J, Cronin MT (eds) (2010) Recent advances in QSAR studies, in series: modern techniques and applications, vol 8. Springer, Netherlands. doi:10.1007/978-1-4020-9783-6
9. Utkov H, Livengood M, Cafiero M (2010) Using density functional theory methods for modeling induction and dispersion interactions in ligand–protein complexes. Ann Rep Comput Chem 6:96–112. doi:10.1016/S1574-1400(10)06007-X
10. Zhang DW, Zhang JZH (2003) Molecular fractionation with conjugate caps for full quantum mechanical calculation of protein–molecule interaction energy. J Chem Phys 119(7):3599–3605. doi:10.1063/1.1591727
11. He X, Mei Y, Xiang Y, Zhang DW, Zhang JZH (2005) Quantum computational analysis for drug resistance of HIV-1 reverse transcriptase to nevirapine through point mutations. Proteins 61(2):423–432. doi:10.1002/prot.20578
12. York DM, Lee T-S (eds) (2009) Multi-scale quantum models for biocatalysis. In: Modern techniques and applications, vol. 7, Springer, Dordrecht. doi:10.1007/978-1-4020-9956-4
13. Mulholland AJ (2007) Chemical accuracy in QM/MM calculations on enzyme-catalysed reactions. Chem Cent J 1(1):19–24. doi:10.1186/1752-153X-1-19
14. Söderhjelm P, Aquilante F, Ryde U (2009) Calculation of protein–ligand interaction energies by a fragmentation approach combining high-level quantum chemistry with classical many-body effects. J Phys Chem B 113(32):11085–11094

15. Senn HM, Thiel W (2009) QM/MM methods for biomolecular systems. Angew Chem Int Ed 48(7):1198–1229. doi:10.1002/anie.200802019
16. de Vivo M (2011) Bridging quantum mechanics and structure-based drug design. Front Biosci 16(1):1619–1633. doi:10.2741/3809
17. Lodola A, de Vivo M (2012) The increasing role of QM/MM in drug discovery. Adv Prot Chem Struct Biol 87:337–362. doi:10.1016/B978-0-12-398312-1.00011-1
18. Cavalli A, Carloni P, Recanatini M (2006) Target-related applications of first principles quantum chemical methods in drug design. Chem Rev 106(9):3497–3519. doi:10.1021/cr050579p
19. Hu L, Söderhjelm P, Ryde U (2013) Accurate reaction energies in proteins obtained by combining QM/MM and large QM calculations. J Chem Theor Comput 9(1):640–649. doi:10.1021/ct3005003
20. Zalesny R, Papadopoulos MG, Mezey PG, Leszczynski J (eds) (2011) Linear-scaling techniques in computational chemistry and physics. In: Challenges advances computational chemistry physics, vol 13. Springer, Dordrecht. doi:10.1007/978-90-481-2853-2
21. Whitten JL (1973) Coulombic potential energy integrals and approximations. J Chem Phys 58(10):4496–4501. doi:10.1063/1.1679012
22. Baerends EJ, Ellis DE, Ros P (1973) Self-consistent molecular Hartree–Fock–Slater calculations I. The computational procedure. Chem Phys 2(1):41–51. doi:10.1016/0301-0104(73)80059-X
23. Dunlap BI, Connolly JWD, Sabin JR (1979) On some approximations in applications of $X\alpha$ theory. J Chem Phys 71(8):3396–3402. doi:10.1063/1.438728
24. Dunlap BI, Connolly JWD, Sabin JR (1979) On first-row diatomic molecules and local density models. J Chem Phys 71(12):4993–4999. doi:10.1063/1.438313
25. Feyereisen M, Fitzgerald G, Komornicki A (1993) Use of approximate integrals in ab initio theory. An application in MP2 energy calculations. Chem Phys Lett 208 359–363. doi:10.1016/0009-2614(93)87156-W
26. Eichkorn K, Weigend F, Treutler O, Ahlrichs R (1997) Auxiliary basis sets for main row atoms and transition metals and their use to approximate Coulomb potentials. Theor Chem Acc 97(1-4):119–124. doi:10.1007/s002140050244
27. Weigend F, Häser M, Patzelt H, Ahlrichs R (1998) RI-MP2: optimized auxiliary basis sets and demonstration of efficiency. Chem Phys Lett 294(1–3):143–152. doi:10.1016/S0009-2614(98)00862-8
28. Furche F, Ahlrichs R, Hättig C, Klopper W, Sierka M, Weigend F (2013) Turbomole. WIREs Comput Mol Sci. doi:10.1002/wcms.1162
29. Neese F (2012) The ORCA program system. WIREs Comput Mol Sci 2(1):73–78. doi:10.1002/wcms.81
30. Aguirre D, Chifotides HT, Angeles-Boza AM, Chouai A, Turro C, Dunbar KR (2009) Redox-regulated inhibition of T7 RNA polymerase via establishment of disulfide linkages by substituted Dppz dirhodium(I, II) complexes. Inorg Chem 48(10):4435–4444. doi:10.1021/ic900164j
31. Villar JAFP, Lima FTD, C.L. Veber, A.R.M. Oliveira, A.K. Calgarotto, S. Marangoni, da Silva SL (2008) Synthesis and evaluation of nitrostyrene derivative compounds, new snake venom phospholipase A2 inhibitors. Toxicon 51(8):1467–1478. doi:10.1016/j.toxicon.2008.03.023
32. Parameswari AR, Kumaradhas P (2013) Exploring the conformation, charge density distribution and the electrostatic properties of galanthamine molecule in the active site of AChE using DFT and AIM theory. Int J Quant Chem 113(8):1200–1208. doi:10.1002/qua.24251
33. Silva JRA, Lameira J, Alves CN (2012) Insights for design of *Trypanosoma cruzi* GAPDH inhibitors: a QM/MM MD study of 1,3-bisphospo-D-glyceric acid analogs. Int J Quant Chem 112(20):3398–3402. doi:10.1002/qua.24253
34. Negri M, Recanatini M, Hartmann RW (2011) Computational investigation of the binding mode of bis(hydroxylphenyl) arenes in 17β-HSD1: molecular dynamics simulations, MM-PBSA free energy calculations, and molecular electrostatic potential maps. J Comp Aid Mol Des 25(9):795–811. doi:10.1007/s10822-011-9464-7

35. Arooj M, Thangapandian S, John S, Hwang S, Park JK, Lee KW (2012) Computational studies of novel chymase inhibitors against cardiovascular and allergic diseases: mechanism and inhibition. Chem Biol Drug Des 80(6):862–875. doi:10.1111/cbdd.12006

36. Muzet N, Guillot B, Jelsch C, Howardt E, Lecomte C (2003) Electrostatic complementarity in an aldose reductase complex from ultra-high-resolution crystallography and first-principles calculations. Proc Nat Acad Sci U S A 100(15):8747. doi:10.1073/pnas.1432955100

37. Van Damme S, Bultinck P (2009) Conceptual DFT properties-based 3D QSAR: analysis of inhibitors of the nicotine metabolizing CYP2A6 enzyme. J Comput Chem 30(12):1749–1757. doi:10.1002/jcc.21177

38. Wan J, Zhang LI, Yang G (2004) Quantitative structure-activity relationships for phenyl triazolinones of protoporphyrinogen oxidase inhibitors: a density functional theory study. J Comput Chem 25(15):1827–1832. doi:10.1002/jcc.20122

39. Zhang L, Hao G-F, Tan Y, Xi Z, Huang M-Z, Yang G-F (2009) Bioactive conformation analysis of cyclic imides as protoporphyrinogen oxidase inhibitor by combining DFT calculations, QSAR and molecular dynamic simulations. Bioorgan Med Chem 17(14):4935–4942. doi:10.1016/j.bmc.2009.06.003

40. Lodola A, Capoferri L, Rivara S, Tarzia G, Piomelli D, Mulholland A, Mor M (2013) Quantum mechanics/molecular mechanics modeling of fatty acid amide hydrolase reactivation distinguishes substrate from irreversible covalent inhibitors. J Med Chem 56(6):2500–2512. doi:10.1021/jm301867x

41. Gueto-Tettay C, Drosos JC, Vivas-Reyes R (2011) Quantum mechanics study of the hydroxyethylamines-BACE-1 active site interaction energies. J Comp Aid Mol Des 25(6):583–597. doi:10.1007/s10822-011-9443-z

42. Evin G, Weidemann A (2002) Biogenesis and metabolism of Alzheimer's disease Abeta amyloid peptides. Peptides 23(7):1285–1297. doi:10.1016/S0196-9781(02)00063-3

43. McGeer PL, McGeer EG (2001) Inflammation, autotoxicity and Alzheimer disease. Neurobiol Aging 22(6):799–809. doi:10.1016/S0197-4580(01)00289-5

44. Zhao Y, Truhlar DG (2008) The M06 suite of density functionals for main group thermochemistry, thermochemical kinetics, noncovalent interactions, excited states, and transition elements: two new functionals and systematic testing of four M06-class functionals and 12 other function. Theor Chem Acc 120(1–3):215–241. doi:10.1007/s00214-007-0310-x

45. Xu X, Goddard WA (2004) From the cover: The X3LYP extended density functional for accurate descriptions of nonbond interactions, spin states, and thermochemical properties. Proc Nat Acad Sci U S A 101(9):2673–2677. doi:10.1073/pnas.0308730100

46. Durrington P (2003) Dyslipidaemia. Lancet 362(9385):717–731. doi:10.1016/S0140-6736(03)14234–1

47. Istvan ES, Deisenhofer J (2001) Structural mechanism for statin inhibition of HMG-CoA reductase. Science 292(5519):1160–1164. doi:10.1126/science.1059344

48. Utkov HE, Price AM, Cafiero M (2011) MP2, density functional theory, and semi-empirical calculations of the interaction energies between a series of statin-drug-like molecules and the HMG-CoA reductase active site. Comp Theor Chem 967(1):171–178. doi:10.1016/j.comptc.2011.04.013

49. Leopoldini M, Malaj N, Toscano M, Sindona G, Russo N (2010) On the inhibitor effects of bergamot juice flavonoids binding to the 3-hydroxy-3-methylglutaryl-CoA Reductase (HMGR) Enzyme. J Agr Food Chem 58(19):10768–10773. doi:10.1021/jf102576j

50. Hebert PR, Gaziano JM, Chan KS, Hennekens CH (1997) Cholesterol lowering with statin drugs, risk of stroke and total mortality. An overview of randomized trials. J Am Med Assoc 278(4):313–321. doi:10.1001/jama.1997.03550040069040

51. Leopoldini M, Marino T, Russo N, Toscano M (2009) Potential energy surfaces for reaction catalyzed by metalloenzymes from quantum chemical computations. In: Russo N, Antonchenko VY, Kryachko ES (eds) Self-organization of molecular systems: from molecules and clusters to nanotubes and proteins, NATO Science for Peace and Security Series A: Chemistry and Biology. Springer, New York, p 275–313. doi:10.1007/978-90-481-2590-6_13

52. Antony J, Gresh N, Olsen L, Hemmingsen L, Schofield CJ, Bauer R (2002) Binding of D- and L-captopril inhibitors to metallo-β-lactamase studied by polarizable molecular mechanics and quantum mechanics. J Comput Chem 23(13):1281–1296. doi:10.1002/jcc.10111

53. Antony J, Piquemal J-P, Gresh N (2005) Complexes of thiomandelate and captopril mercaptocarboxylate inhibitors to metallo-beta-lactamase by polarizable molecular mechanics. Validation on model binding sites by quantum chemistry. J Comput Chem 26(11):1131–1147. doi:10.1002/jcc.20245

54. Chen X, Gao F, Zhou Z-X, Yang W-Y, Guo L-T, Ji L-N (2010) Effect of ancillary ligands on the topoisomerases II and transcription inhibition activity of polypyridyl ruthenium(II) complexes. J Inorg Biochem 104(5):576–582. doi:10.1016/j.jinorgbio.2010.01.010

55. Casini A, Edafe F, Erlandsson M, Gonsalvi L, Ciancetta A, Re N, Ienco A, Messori L, Peruzzini M, Dyson PJ (2010) Rationalization of the inhibition activity of structurally related organometallic compounds against the drug target cathepsin B by DFT. Dalton Trans 39(23):5556–5563. doi:10.1039/c003218b

56. Shokhen M, Khazanov N, Albeck A (2011) The mechanism of papain inhibition by peptidyl aldehydes. Proteins 79(3):975–985. doi:10.1002/prot.22939

57. Greig NH, Sambamurti K, Yu Q, Brossi A, Bruinsma GB, Lahiri DK (2005) An overview of phenserine tartrate, a novel acetylcholinesterase inhibitor for the treatment of Alzheimer's disease. Curr Alzheimer Res 2(3):281–290. doi:10.2174/1567205054367829

58. Lahiri DK, Farlow MR, Hintz N, Utsuki T, Greig NH (2000) Cholinesterase inhibitors, beta-amyloid precursor protein and amyloid beta-peptides in Alzheimer's disease. Acta Neurol Scand 102(s176):60–67. doi:10.1034/j.1600-0404.2000.00309.x

59. Leader H, Wolfe AD, Chiang PK, Gordon RK (2002) Pyridophens: binary pyridostigmine-aprophen prodrugs with differential inhibition of acetylcholinesterase, butyrylcholinesterase, and muscarinic receptors. J Med Chem 45(4):902–910. doi:10.1021/jm010196t

60. Yu Q, Holloway HW, Flippen-Anderson JL, Hoffman B, Brossi A, Greig NH (2001) Methyl analogues of the experimental Alzheimer drug phenserine: synthesis and structure/activity relationships for acetyl- and butyrylcholinesterase inhibitory action. J Med Chem 44(24):4062–4071. doi:10.1021/jm010080x

61. Correa-Basurto J, Flores-Sandoval C, Marín-Cruz J, Rojo-Domínguez A, Espinoza-Fonseca LM, Trujillo-Ferrara JG (2007) Docking and quantum mechanic studies on cholinesterases and their inhibitors. Eur J Med Chem 42(1):10–19. doi:10.1016/j.ejmech.2006.08.015

62. Zhang Y, Kua J, McCammon JA (2002) Role of the catalytic triad and oxyanion hole in acetylcholinesterase catalysis: an ab initio QM/MM study. J Am Chem Soc 124(35):10572–10577. doi:10.1021/ja020243m

63. Nascimento ECM, Martins JBL, dos Santos ML, Gargano R (2008) Theoretical study of classical acetylcholinesterase inhibitors. Chem Phys Lett 458(4–6):285–289. doi:10.1016/j.cplett.2008.05.006

64. Khan MAS, Lo R, Bandyopadhyay TT, Ganguly BB (2011) Probing the reactivation process of sarin-inhibited acetylcholinesterase with α-nucleophiles: hydroxylamine anion is predicted to be a better antidote with DFT calculations. J Mol Graph Model 29(8):1039–1046. doi:10.1016/j.jmgm.2011.04.009

65. Khan MAS, Ganguly B (2012) Assessing the reactivation efficacy of hydroxylamine anion towards VX-inhibited AChE: A computational study. J Mol Model 18(5):1801–1808. doi:10.1007/s00894-011-1209-y

66. Shi Y-B, Fu L, Hasebe T, Ishizuya-Oka A (2007) Regulation of extracellular matrix remodeling and cell fate determination by matrix metalloproteinase stromelysin-3 during thyroid hormone-dependent post-embryonic development. Pharmacol Therapeut 116(3):391–400. doi:10.1016/j.pharmthera.2007.07.005

67. Smith MF, Ricke WA, Bakke LJ, Dow MPD, Smith GW (2002) Ovarian tissue remodeling: role of matrix metalloproteinases and their inhibitors. Mol Cell Endocrinol 191(1):45–56. doi:10.1016/S0303-7207(02)00054-0

68. Kawasaki Y, Xu Z-Z, Wang X, Park JY, Zhuang Z-Y, Tan P-H, Gao Y-J, Roy K, Corfas G, Lo EH, Ji R-R (2008) Distinct roles of matrix metalloproteases in the early- and late-phase development of neuropathic pain. Nat Med 14(3):331–336. doi:10.1038/nm1723

69. Egeblad M, Werb Z (2002) New functions for the matrix metalloproteinases in cancer progression. Nat Rev Cancer 2(3):161–174. doi:10.1038/nrc745

70. Noël A, Jost M, Maquoi E (2008) Matrix metalloproteinases at cancer tumor–host interface. Semin Cell Dev Biol 19(1):52–60. doi:10.1016/j.semcdb.2007.05.011

71. Tao P, Fisher JF, Shi Q, Mobashery S, Schlegel HB (2010) Matrix metalloproteinase 2 (MMP2) inhibition: DFT and QM/MM studies of the deprotonation-initialized ring-opening reaction of the sulfoxide analogue of SB-3CT. J Phys Chem B 114(2):1030–1037. doi:10.1021/jp909327y

72. Tao P, Fisher JF, Shi Q, Vreven T, Mobashery S, Schlegel HB (2009) Matrix metalloproteinase 2 inhibition: combined quantum mechanics and molecular mechanics studies of the inhibition mechanism of (4-phenoxyphenylsulfonyl)methylthiirane and its oxirane analogue. Biochemistry 48(41):9839–9847. doi:10.1021/bi901118r

73. Augé F, Hornebeck W, Decarme M, Laronze J-Y (2003) Improved gelatinase a selectivity by novel zinc binding groups containing galardin derivatives. Bioorg Med Chem Lett 13(10):1783–1786. doi:10.1016/S0960-894X(03)00214-2

74. Rouffet M, Denhez C, Bourguet E, Bohr F, Guillaume D (2009) In silico study of MMP inhibition. Org Biomol Chem 7(18):3817–3825. doi:10.1039/b910543c

75. Li D, Zheng Q, Fang X, Ji H, Yang J, Zhang H (2008) Theoretical study on potency and selectivity of novel non-peptide inhibitors of matrix metalloproteinases MMP-1 and MMP-3. Polymer 49(15):3346–3351. doi:10.1016/j.polymer.2008.05.026

76. da Silva SL, Calgarotto AK, Maso V, Damico DC, Baldasso P, Veber CL, Villar JAFP, Oliveira ARM, Comar M, Oliveira KMT, Marangoni S (2009) Molecular modeling and inhibition of phospholipase A2 by polyhydroxy phenolic compounds. Eur J Med Chem 44(1):312–321. doi:10.1016/j.ejmech.2008.02.043

77. Šramko M, Garaj V, Remko M (2008) Thermodynamics of binding of angiotensin-converting enzyme inhibitors to enzyme active site model, J Mol Struct—Theochem 869(1–3):19–28. 10.1016/j.theochem.2008.08.018

78. Opie LH, Gersh BJ (2009) Drugs for the Heart. WB Saunders, Philadelphia

79. Lorthiois E, Bernardelli P, Vergne F, Oliveira C, Mafroud A-K, Proust E, Heuze L, Moreau F, Idrissi M, Tertre A, Bertin B, Coupe M, Wrigglesworth R, Descours A, Soulard P, Berna P (2004) Spiroquinazolinones as novel, potent, and selective PDE7 inhibitors. Part 1. Bioorg Med Chem Lett 14(18):4623–4626. doi:10.1016/j.bmcl.2004.07.011

80. Bernardelli P, Lorthiois E, Vergne F, Oliveira C, Mafroud A-K, Proust E, Pham N, Ducrot P, Moreau F, Idrissi M, Tertre A, Bertin B, Coupe M, Chevalier E, Descours A, Berlioz-Seux F, Berna P, Li M (2004) Spiroquinazolinones as novel, potent, and selective PDE7 inhibitors. Part 2: Optimization of 5,8-disubstituted derivatives. Bioorg Med Chem Lett 14(18):4627–4631. doi:10.1016/j.bmcl.2004.07.010

81. Daga PR, Doerksen RJ (2008) Stereoelectronic properties of spiroquinazolinones in differential PDE7 inhibitory activity. J Comput Chem 29(12):1945–1954. doi:10.1002/jcc.20960

82. Horenstein BA, Schramm VL (1993) Correlation of the molecular electrostatic potential surface of an enzymatic transition state with novel transition-state inhibitors. Biochemistry 32(38):9917–9925. doi:10.1021/bi00089a007

83. Braunheim BB, Miles RW, Schramm VL, Schwartz SD (1999) Prediction of inhibitor binding free energies by quantum neural networks. Nucleoside analogues binding to trypanosomal nucleoside hydrolase. Biochemistry 38(49):16076–16083. doi:10.1021/bi990830t

84. Ehrlich JI, Schramm VL (1994) Electrostatic potential surface analysis of the transition state for AMP nucleosidase and for formycin 5'-phosphate, a transition-state inhibitor. Biochemistry 33(30):8890–8896. doi:10.1021/bi00196a005

85. Debnath AK (2013) Rational design of HIV-1 entry inhibitors. In: Kortagere S (ed) Methods in molecular biology. Springer, Clifton, p 185–204. doi:10.1007/978-1-62703-342-8_13

86. Świderek K, Martí S., Moliner V (2012) Theoretical studies of HIV-1 reverse transcriptase inhibition. Phys Chem Chem Phys 14(36):12614–12624. doi:10.1039/c2cp40953d

87. Liang YH, Chen FE (2007) ONIOM DFT/PM3 calculations on the interaction between dapivirine and HIV-1 reverse transcriptase, a theoretical study. Drug Discov Ther 1(1):57–60.

88. Garrec J, Sautet P, Fleurat-Lessard P (2011) Understanding the HIV-1 protease reactivity with DFT: what do we gain from recent functionals?. J Phys Chem B 115(26):8545–8558. doi:10.1021/jp200565w

89. Garrec J, Cascella M, Rothlisberger U, Fleurat-Lessard P (2010) Low inhibiting power of N⋯CO based peptidomimetic compounds against HIV-1 protease: insights from a QM/MM study. J Chem Theor Comput 6(4):1369–1379. doi:10.1021/ct9004728

90. Gautier A, Pitrat D, Hasserodt J (2006) An unusual functional group interaction and its potential to reproduce steric and electrostatic features of the transition states of peptidolysis. Bioorg Med Chem 14(11):3835–3847. doi:10.1016/j.bmc.2006.01.031

91. Waibel M, Hasserodt J (2008) Diversity-oriented synthesis of a drug-like system displaying the distinctive N→C=O interaction. J Org Chem 73(16):6119–6126. doi:10.1021/jo800719j

92   Waibel M, Pitrat D, Hasserodt J (2009) On the inhibition of HIV-1 protease by hydrazino-ureas displaying the N→C=O interaction. Bioorg Med Chem 17(10):3671–3679. doi:10.1016/j.bmc.2009.03.059

93. Park C, Koh JS, Son YC, Choi H, Lee CS, Choy N, Moon KY, Jung WH, Kim SC, Yoon H (1995) Rational design of irreversible, pseudo-C2-symmetric hiv-1 protease inhibitors. Bioorg Med Chem Lett 5(16):1843–1848. doi:10.1016/0960-894X(95)00306-E

94. Lee CS, Choy N, Park C, Choi H, Son YC, Kim S, Ok JH, Yoon H, Kim SC (1996) Design, synthesis, and characterization of dipeptide isostere containing cis-epoxide for the irreversible inactivation of HIV protease. Bioorg Med Chem Lett 6(6):589–594. doi:10.1016/0960-894X(96)00087-X

95. Choy N, Choi H, Jung WH, Kim CR, Yoon H, Kim SC, Lee TG, Koh JS (1997) Synthesis of irreversible HIV-1 protease inhibitors containing sulfonamide and sulfone as amide bond isosteres. Bioorg Med Chem Lett 7(20):2635–2638. doi:10.1016/S0960-894X(97)10054-3

96. Kóňa J (2008) Theoretical study on the mechanism of a ring-opening reaction of oxirane by the active-site aspartic dyad of HIV-1 protease. Org Biomol Chem 6(2):359–365. doi:10.1039/b715828a

97. Pommier Y, Johnson AA, Marchand C (2005) Integrase inhibitors to treat HIV/AIDS. Nat Rev Drug Discov 4(3):236–248. doi:10.1038/nrd1660

98. Ingale KB, Bhatia MS (2011) HIV-1 integrase inhibitors: a review of their chemical development. Antivir Chem Chemoth 22(3):95–105. doi:10.3851/IMP1740

99. Messiaen P, Wensing AMJ, Fun A, Nijhuis M, Brusselaers N, Vandekerckhove L (2013) Clinical use of HIV integrase inhibitors: a systematic review and meta-analysis. PloS One 8(1):e52562. doi:10.1371/journal.pone.0052562

100. Liao C, Nicklaus MC (2010) Tautomerism and magnesium chelation of HIV-1 integrase inhibitors: a theoretical study. Chem Med Chem 5(7):1053–1066. doi:10.1002/cmdc.201000039

101. Agrawal A, DeSoto J, Fullagar JL, Maddali K, Rostami S, Richman DD, Pommier Y, Cohen SM (2012) Probing chelation motifs in HIV integrase inhibitors. Proc Nat Acad Sci U S A 109(7):2251–2256. doi:10.1073/pnas.1112389109

102. Thalheim T, Vollmer A, Ebert R-U, Kühne R, Schüürmann G (2010) Tautomer identification and tautomer structure generation based on the InChI code. J Chem Inf Model 50(7):1223–1232. doi:10.1021/ci1001179

103. Nunthaboot N, Pianwanit S, Parasuk V, Kokpol S, Wolschann P (2007) Theoretical study on the HIV-1 integrase inhibitor 1-(5-chloroindol-3-yl)-3-hydroxy-3-(2H-tetrazol-5-yl)-propenone (5CITEP). J Mol Struct 844–845:208–214. doi:10.1016/j.molstruc.2007.06.026

104. Alves CN, Martí S, Castillo R, Andrés J, Moliner V, Tuñón I, Silla E (2007) Calculation of binding energy using BLYP/MM for the HIV-1 integrase complexed with the S-1360 and two analogues. Bioorgan Med Chem 15(11):3818–3824. doi:10.1016/j.bmc.2007.03.027

105. Lespade L, Bercion S (2010) Theoretical study of the mechanism of inhibition of xanthine oxidase by flavonoids and gallic acid derivatives. J Phys Chem B 114(2):921–928. doi:10.1021/jp9041809

106. Lin C-M, Chen C-S, Chen C-T, Liang Y-C, Lin J-K (2002) Molecular modeling of flavonoids that inhibits xanthine oxidase. Biochem Biophys Res Commun 294(1):167–172. doi:10.1016/S0006-291X(02)00442-4

107. Hall LH, Kier LB (1995) Electrotopological state indices for atom types: a novel combination of electronic, topological, and valence state information,. J Chem Inf Model 35(6):1039–1045. doi:10.1021/ci00028a014

108. Fogliani B, Raharivelomanana P, Bianchini J-P, Bouraïma-Madjèbi S, Hnawia E (2005) Bioactive ellagitannins from *Cunonia macrophylla*, an endemic Cunoniaceae from New Caledonia. Phytochemistry 66(2):241–247. doi:10.1016/j.phytochem.2004.11.016

109. Fenton JW, Ofosu FA, Moon DG, Maraganore JM (1991) Thrombin structure and function: why thrombin is the primary target for antithrombotics. Blood Coagul Fibrin 2(1):69–75.

110. Alzate-Morales JH, Contreras R, Soriano A, Tuñón I, Silla E (2007) A computational study of the protein-ligand interactions in CDK2 inhibitors: using quantum mechanics/molecular mechanics interaction energy as a predictor of the biological activity. Biophys J 92:430–439. doi:10.1529/biophysj.106.091512

111. De Oliveira EB, Humeau C, Maia ER, Chebil L, Ronat E, Monard G, Ruiz-Lopez MF, Ghoul M, Engasser J-M (2010) An approach based on Density Functional Theory (DFT) calculations to assess the candida antarctica lipase B selectivity in rutin, isoquercitrin and quercetin acetylation. J Mol Catal B—Enzym 66(3–4):325–331. doi:10.1016/j.molcatb.2010.06.009

112. Benini S, Rypniewski WR, Wilson KS, Ciurli S, Mangani S (2001) Structure-based rationalization of urease inhibition by phosphate: novel insights into the enzyme mechanism. J Biol Inorg Chem 6(8):778–790. doi:10.1007/s007750100254

113. Karplus PA, Pearson MA, Hausinger RP (1997) 70 Years of crystalline urease: what have we learned?. Acc Chem Res 30(8):330–337. doi:10.1021/ar960022j

114. Leopoldini M, Marino T, Russo N, Toscano M (2008) On the binding mode of urease active site inhibitors: a density functional study. Int J Quant Chem 108(11):2023–2029. doi:10.1002/qua.21758

115. Wei D, Lei B, Tang M, Zhan C-G (2012) Fundamental reaction pathway and free energy profile for inhibition of proteasome by epoxomicin. J Am Chem Soc 134(25):10436–10450. doi:10.1021/ja3006463

116. Weigend F (2008) Hartree–Fock exchange fitting basis sets for H to Rn. J Comput Chem 29(2):167–175. doi:10.1002/jcc.20702

117. Neese F, Wennmohs F, Hansen A, Becker U (2009) Efficient, approximate and parallel Hartree–Fock and hybrid DFT calculations. A "chain-of-spheres" algorithm for the Hartree–Fock exchange. Chem Phys 356(1–3):98–109. 10.1016/j.chemphys.2008.10.036

118. Ferrer S, Ruiz-Pernía J, Martí S et al (2011) Hybrid schemes based on quantum mechanics/molecular mechanics simulations goals to success, problems, and perspectives. Adv Protein Chem Struct Biol 85:81–142. doi:10.1016/B978-0-12-386485-7.00003-X